Nuclear Lamina binds the EBV genome during latency and regulates viral gene expression

Lisa Beatrice Caruso[1], Rui Guo[2-4], Sarah Boyle[1], Kelsey Keith[5], Jozef Madzo[5], Jason Wasserman[6], Andrew Kossenkov[1], Benjamin E. Gewurz[2-4] and Italo Tempera[1#].

1 The Wistar Institute, Philadelphia, PA 19104

2 Division of Infectious Diseases, Brigham & Women's Hospital, Boston, MA 02115

3 Department of Microbiology, Harvard Medical School, Boston, MA 02115

4 Broad Institute of Harvard and MIT, Cambridge, MA 02142

5 The Coriell Institute for Medical Research, Camden, NJ 08103

6 The Fels Cancer Institute for Personalized Medicine, School of Medicine Temple University, Philadelphia, PA 19140

#Address correspondence to Italo Tempera, itempera@wistar.org

ABSTRACT

The Epstein Barr virus (EBV) establishes a persistent latent infection in almost 90% of the population worldwide. EBV latent infection is associated with several malignancies of epithelial and lymphoid origin. In latently infected cells, the EBV genome persists as a chromatinized episome that expresses a limited set of viral genes. Latent genes are expressed in different patterns that are referred to as latency types. Latency types coincide with varying stages of EBV infection and various malignancies. Our previous work demonstrated that latency types correlate with differences in the composition and structure of the EBV episome. Several cellular factors, including nuclear lamina, regulate chromatin composition and chromatin architecture. The interaction with nuclear lamina has already been studied in the context of EBV lytic reactivation. Still, the role of nuclear lamina in controlling EBV latency has not been investigated. Here, we reported that nuclear lamina is also another essential epigenetic regulator of the EBV episome. First, we observed that in B cells, EBV infection affects the composition of nuclear lamina by inducing the expression of Lamin A/C, and Lamin A/C is present only in EBV+ B cells expressing the Type III latency program. By ChIP-seq, we determined that lamins, Lamin B1 and Lamin A/C, bind the EBV genome, and their binding correlates with deposition of the histone repressive mark H3K9me2. By RNA-seq, we observed that the knock-out of Lamin A/C alters EBV gene expression in B cells and decreases H3K9me2 levels across the viral genome. Our data indicate that the interaction between lamins and the EBV episome contributes to the epigenetic control of viral genes expression during latency, suggesting a restrictive function of the nuclear lamina in the host response against the intrusion of viral DNA into the nucleus.

36 **AUTHOR SUMMARY**

37 Epstein-Barr virus (EBV) is a common herpesvirus that establishes lifelong latent infection in
38 a small fraction of the B cells of infected individuals. In most cases, EBV infection is asymptomatic;
39 however, especially in the context of immune suppression, EBV latent infection is associated with
40 several malignancies. In EBV+ cancer cells, latent viral gene expression plays an essential role
41 in sustaining the cancer phenotype. In previous works, we and others established that epigenetic
42 modifications of the viral genomes are critical to regulating EBV gene expression during latency.
43 Understanding how the EBV genome is epigenetically regulated during latent infection can help
44 us develop new specific therapeutic targets for treating EBV+ malignancies. Nuclear Lamina plays
45 an essential role in regulating the composition and the structure of cellular chromatin. In the
46 present study, we determined that Nuclear Lamina binds the EBV genome during latency,
47 influencing viral gene expression in the present study. Depleting one component of the nuclear
48 lamina, Lamin A/C, increases the expression of latent EBV genes that are usually associated with
49 cellular proliferation, indicating that the binding of the nuclear lamina with the viral genome is
50 essential to control viral gene expression in infected cells. Our data show for the first time that the
51 nuclear lamina may be involved in the cellular response against EBV infection by restricting viral
52 gene expression.

53 **INTRODUCTION**

54 Epstein Barr Virus (EBV) is a human gamma-herpesvirus highly present worldwide; it's
55 estimate it can affect almost 95% of the population [1-4]. EBV is known as the cause of infectious
56 mononucleosis, and it is also associated with various malignant diseases such as Burkitt
57 lymphoma, Hodgkin's lymphoma, gastric cancer, and nasopharyngeal carcinoma [5-9] . EBV can
58 infect both epithelial and B cells in either a latent or lytic state [10-13]. The latent infection is a
59 strategy adopted by EBV to remain indefinitely and undisturbed in the host, evading the host

60 immune surveillance, in this state, the virus genome can persist as a multicopy nuclear episomes
61 [14, 15]. Moreover, EBV-induced B cell transformation is driven by a few viral proteins that induce
62 transformation and proliferation[16]. Transformation occurs while the virus is in a latent, not lytic,
63 state. During latent infection, EBV can express different pattern of viral genes – referred as latency
64 types – that induce different responses in the infected cells [1, 12, 17-20]

65 Type III latency is characterized by the expression of genes that are necessary to induce B-
66 cell activation and proliferation, all the EBV latent proteins are expressed, among these we have
67 the six nuclear antigens (EBNA1, EBNA2, EBNA3A, EBNA3B, EBNA3C and EBNA-LP), and
68 three membrane proteins (LMP1, LMP2A and LMP2B). Type I is characterized by the expression
69 of only the viral protein EBNA1, which is necessary for viral DNA replication and episome
70 maintenance by tethering the EBV genome to host chromosomes. Switching between different
71 latency types is an essential strategy for EBV to persist in the host and evade immune detection.
72 those epigenetic modifications and chromatin modifying enzymes play an important role in latency
73 switching during EBV latency [13].

74 The EBV-host interaction plays a crucial role in EBV latency switching and many elements
75 can be involved in this reciprocation. Indeed, We and other have previously reported the
76 importance of histone modifications [21-23] [24]and chromatin three-dimensional organization of
77 the EBV genome in the regulation of viral gene expression during latency [21, 25-28]. Several
78 studies have revealed that in eukaryotes, chromatin composition and chromatin structure can be
79 influenced by their interaction of genomic region with the nuclear lamina. These interactions occur
80 through regions of chromatin called lamina-associated domains (LADs)[29-31]. LADs are
81 considered to be regions that have the ability to interact with the lamina, but do not necessarily
82 do so at all times [32, 33]. When LADs are localized to the nuclear periphery, their genes are
83 often poorly expressed and their chromatin is strongly associated with repressive heterochromatin
84 marks such as H3K9me2 [34-36]. Thus, processes that associate LADs with the nuclear periphery

are expected to downregulate gene expression of LAD regions but also can also play a role in other nuclear functions that require the rearrangement of the chromatin structure, for example, DNA replication and repair [37].

The nuclear lamina (NL) is a filamentous protein network at the nuclear periphery formed by proteins known as lamins. These proteins can be grouped into two different families: type A and B lamins and this classification is based on their sequence homologies and molecular weights. Lamins B (B1 and B2) are ubiquitously expressed in every mammalian cell at each stage of differentiation by two different genes (LMNB1 and LMNB2). While lamins A (A and C) are encoded by the same gene (LMNA) who is differently spliced, and they are expressed only in differentiated cells. These protein families are also different with respect to their cellular localization, while B lamins localize only at the nuclear periphery, A and C lamins are present also at the nuclear interior [38-43].

Several groups have demonstrated that nuclear lamins play an antiviral role during replication of herpesviruses, including EBV, HSV1 and HSV2, and HCMV, by functioning as a physical barrier that prevents the egress of viral capsid. Herpesviruses code for viral proteins that target nuclear lamina during lytic infection. For example, the EBV protein BGLF4 is a viral kinase that interacts with the nuclear lamina and cause nuclear lamina degradation by phosphorylation of Lamin A [44-50]. These results clearly underscore the anti-viral role of nuclear lamina during lytic infection. However, whether the nuclear lamina plays an antiviral role also during EBV latency is still unknown. Here, we investigated the role of nuclear lamins in the control of the EBV latency states and its function as epigenetic regulator of the different EBV genes expression profiles observed.

We found that infection of B cells with EBV changes nuclear lamina composition by inducing Lamin A/C expression. We observed also that expression of Lamin A/C is maintained during Type III latency but is lost in Type I latency. We found as consequence of these changes that in Type I

109 Lamin B1 binds several regions of the EBV genome while in Type III cells Lamin A/C binds only
110 a few regulatory viral regions. We observed that regions of the EBV genome repressed by nuclear
111 lamina binding were enriched for the repressive histone mark H3K9me2. Finally, we found that in
112 Type III, knock-out of Lamina A/C or inhibition of H2K9me2 deposition increases EBV gene
113 expression.

114 Altogether, our data suggest that nuclear lamins contribute to the epigenetic control of EBV genes
115 expression during latency by changing the interaction of the host structural proteins with key
116 regulatory regions in the viral genome and important for the mechanisms that regulates the
117 different latency profile.

118 **RESULTS**

119 **Lamin A/C is expressed only in EBV+ cells adopting the Type III latency program.** The role
120 of the nuclear lamina during lytic infection of herpesviruses has been well documented, it has
121 been shown that herpesviruses code for lytic proteins that interact with and modify nuclear lamin
122 during reactivation to promote viral egress [50]. Instead, the role of the nuclear lamina during
123 latent infection of herpes viruses has been explored less. We assessed the expression of the two
124 major components of the nuclear lamina, Lamin B1 and Lamin A/C, in B cells from a healthy donor
125 and in a panel of EBV+ and EBV- B cell lines (**Figure 1**). Using western blot analysis, we observed
126 that Lamin B1 is expressed in all cell lines regardless of either EBV+ status or the type of latency
127 (**Figure 1A**). Instead, we noticed, a clear link between Lamin A/C expression and latency type in
128 the EBV-positive cell lines. The Type III latency cells (Mutu-LCL, B95.8-LCL, GM12878 and Mutu
129 III) expressed Lamin A/C (**Figure 1A**), whereas Type I latency cells (Mutu I) did not. These data
130 show that the expression of Lamin A/C is strongly associated to the Type III viral latency type.
131 Because the Mutu I (Type I) and Mutu III (Type III) cell lines are fully isogenic with respect to both
132 the host and EBV genomes, the difference in Lamin A/C expression in different EBV latency types

133 were not due to inherent genetic differences in the host cells or EBV strains. Lamin A/C expression
134 was absent also in primary B cells.

135 Next, we assessed by immunofluorescence microscopy, the specific localization of Lamin B1 and
136 Lamin A/C in the nucleus in EBV+ Mutu I and Mutu-LCL cells. We observed that, as expected,
137 Lamin B1 was localized at the nuclear periphery and, in particular, at the nuclear rim in both cell
138 lines (**Figure 1B**). We detected Lamin A/C in LCL but not in Mutu I cells, confirming that only Type
139 III EBV+ B cells express Lamin A/C (**Figure 1B**). In LCLs, Lamin A/C staining was distributed
140 around the nuclear rim and overlapped with Lamin B1 staining (**Figure 1C**). Moreover, in LCL
141 Lamin A/C staining was present also in the nucleoplasm, although the staining intensity was lower
142 that the staining intensity at the nuclear rim (**Figure 1C**). These results are consistent with a
143 previous report indicating that a fraction of Lamin A/C exists in the nucleoplasm[42]. Overall, these
144 results demonstrated that Lamin A/C expression is linked to EBV infection and in particular to the
145 Type III EBV latency.

146 **EBV infection of primary B cells induces Lamin A/C expression.** The previous results
147 indicated that Lamin A/C expression is linked to EBV latent infection of B cells. Thus, we next
148 asked whether Lamin A/C is induced upon EBV infection of primary B cells, or whether Lamin A/C
149 expression is induced as a later consequence of infection. To assess the kinetics of Lamin A/C
150 expression following EBV infection, we assessed by immunofluorescence microscopy Lamin A/C
151 expression in primary B cells from a healthy human donor, before and during the 48 hours after
152 infection with EBV. We observed that Lamin A/C is upregulated in B cells newly infected with
153 EBV, at both RNA and protein levels just after 7 days post infection (**Figure 2A**), and that Lamin
154 A/C stain localized at both the nuclear rim and the nucleoplasm (**Figure 2A**). The intensity of
155 Lamin A/C staining in the nucleoplasm was higher compared to that observed in latently infected
156 cells (**Figure 1C**). In infected B cells, Lamin B1 and Lamin A/C staining showed several

157 invaginations of the nuclear membrane compared to uninfected B cells, which resulted in a shape
158 of the nuclei being less spherical and more irregular (**Figure 2A**).

159 Once we established that EBV infection is sufficient to induce expression of Lamin A/C, we
160 asked how Lamin A/C expression changes during the progression of EBV infection. It has been
161 reported that both viral and cellular genes are expressed in different patterns during the time
162 necessary for EBV to transform infected primary B cells into LCLs. Therefore, we interrogated
163 RNAseq data collected from triplicate healthy donor primary B cell samples at rest and at 9
164 timepoints following EBV infection [51] (**Figure 2B**). Interestingly, Lamin A/C mRNA abundance
165 increased by day 7 post-EBV infection, a timepoint when latency III proteins are detectable by
166 immunoblot [52]. Several latency III proteins increase in abundance at later timepoints, in
167 particular LMP1 [52-54], and LMNA mRNA levels were further upregulated through day 28 days
168 post-infection, when EBV+ B cells exhibit LCL physiology (**Figure 2B**). Overall, Lamina A/C
169 expression levels increased ~10-fold between uninfected B cells and day 28-day post infection
170 (**Figure 2B**). To further confirm that the increase in Lamin A/C expression at the transcriptional
171 level corresponds to an increase in the Lamin A/C protein level at these timepoints, we utilized
172 proteomic data obtained from human primary B-cells at the same timepoints [52]. The increase in
173 Lamin A/C protein expression mirrored the increase in Lamin A/C mRNA expression, with a ~5-
174 fold increase in Lamin A/C protein expression in B cells (**Figure 2C**). Overall, these results
175 demonstrate that primary infection of EBV and the subsequent establishment of the Type III
176 latency program induce Lamin A/C expression in B cells.

177 **Activation of B cells induces Lamin A/C expression.** In B cells, EBV Type III latency mimics
178 key aspects of antigen-mediated activation, begging the question of whether physiological
179 activation of B cells also induces Lamin A/C expression. To address this question, we assessed
180 by immunofluorescence microscopy Lamin A/C and Lamin B1 expression in primary B cells before
181 and after a 48-hour activation with: Interleukin 4 (IL4 20 ng/mL), CD40 ligand (CD40L 5uM), and

182 CpG oligodeoxynucleotides (25 ng/mL) (**Figure 3A**). We sorted activated B cells by flow
183 cytometry for CD69 and analyzed cells by microscopy. As expected, Lamin B1 staining remained
184 unaltered after B cell activation, whereas Lamin A/C could be detected in B cells only after
185 activation (**Figure 3A**). We observed that the Lamin A/C staining was present at the nuclear rim
186 and overlapped with Lamin B1 staining; only minimal Lamin A/C staining was observed in the
187 nucleoplasm (**Figure 3A**). In addition activated B cell nuclear morphology differed from that of
188 control cells. In control cells, the nuclear membrane had a smooth, circular shape without
189 significant invaginations (**Figure 3A**). Instead, in the activated cells, which tended to cluster
190 together, the nuclear membrane had an irregular and elongate shape, with the presence of some
191 invaginations along the nuclear rim (**Figure 3A**). To gain insights into how these B-cell stimuli
192 alter expression of Lamin A/C either alone or in combination, we used RNA-Seq and proteomic
193 analyses. Activation of B cells by CD40L alone, or in combinations with either CpG, or IgM, or
194 IL4, rapidly induced Lamin A/C expression (**Figure 3B**). Interestingly, the EBV oncoprotein LMP1
195 mimics signaling from activated CD40 receptors [55, 56] indicating that CD40 signaling pathway
196 is important for Lamin A/C induction. Next, we determined whether the observed changed in
197 Lamin A/C mRNA expression induced by CD40L activation resulted in increased levels of Lamin
198 A/C protein. We found that CD40, alone or in combination with other activators, was able to induce
199 the expression of Lamin A/C also at the protein levels (**Figure 3C**). These results indicated that
200 induction of Lamin A/C is part of the cascade of cellular changes that occur in B cells after
201 particular types of activation, in particular by T-cell CD40L stimulation.

202 **The EBV genome interacts with the nuclear lamina during latency**. Nuclear lamina and
203 lamins, in particular Lamin A/C, play an important role in transcription by regulating the chromatin
204 composition and the chromatin structure of genomic regions localized at the nuclear periphery.
205 Since Lamin A/C is expressed in B cells following EBV infection and in cell lines that adopt the
206 Type III latency program, we decided to investigate whether the EBV genome interacts with the

207 nuclear lamina and how Lamin A/C expression may affect any such interaction. To determine if
208 the EBV genome interacts with the nuclear lamina we analyzed Lamin B1 occupancy across the
209 viral episome by chromatin immunoprecipitation followed by next-generation sequencing, ChIP-
210 Seq (**Figure 4**). We performed Lamin B1 ChIP-Seq in Mutu I cells (as a model of Type I Latency)
211 and LCL (as a model of Type III latency) and then compared the Lamin B1 occupancy across the
212 EBV genome in these two cells lines. In Type I Mutu I cells, a large portion of the viral genome
213 was associated with Lamin B1 (**Figure 4A**). In particular, most of the binding sites for Lamin B1
214 were localized at different regions of the EBV genome that are fundamental for regulating the
215 expression of EBV latent genes. In particular, we observed Lamin B1 occupancy at the region
216 between ~35 kb-50kb downstream of the terminal repeat that encodes EBNA2 and also
217 encompasses one of the EBV origins of lytic replication, *oriLyt R*. Notably, we previously identified
218 a CTCF binding site in this region, just upstream of the viral Q promoter (Qp) [26, 57]. Qp is the
219 only latency gene promoter active in the Type I program. Lamin B1 occupies sites in the region
220 where the Z promoter (Zp) for the lytic cycle activator immediate-early gene *BZLF1*. Lamin B1
221 also highly occupied the viral genome at regions encoding viral microRNAs around position 150
222 kb as well as at the terminal repeat (TR) region (**Figure 4A**). In contrast to Mutu I cells with type
223 I latency, in LCL cells, very few regions of the EBV genome were occupied by Lamin B1 (**Figure**
224 **4A**). Interesting, the regions of EBV genome that were occupied by Lamin B1 in LCL cells were
225 were also occupied by Lamin B1 in Mutu I, including the region at ~35 kb (coding for EBNA2),
226 and the TR regions. Overall, these results indicate that the EBV genome interacts with Lamin B1
227 more in Type I latently infected cells that in Type III cells.

228 **Lamin A/C interacts with the EBV genome in EBV+ cells adopting the Type III latency type.**
229 The previous results indicated that Lamin B1 occupancy across the EBV genome differed
230 between latency types. Since Type III latently infected cells expressed Lamin A/C, we
231 hypothesized that in Type III cells the viral genome would associate with Lamin A/C, rather than

232 Lamin B1. We used ChIP-seq to assess Lamin A/C occupancy across the EBV genome in LCLs
233 (**Figure 4A**). Lamin A/C bound the EBV genome at only a few loci, including the TR regions and
234 the Zp promoter (**Figures 4A and 4B**). To determine if Lamin A/C and Lamin B1 co-occupy
235 genomic sites in LCLs, we overlaid the Lamin A/C and Lamin B1 ChIP-seq tracks. We found that
236 both Lamin A/C and Lamin B1 bind at the TR region and the region which codes for a portion of
237 EBNA2, located around ~35 kb of viral genome (**Figures 4A and 4B**). Next, we determined
238 whether the regions of the EBV genome that are associated with Lamin A/C in LCLs are bound
239 by Lamin B1 in Mutu I cells. When we aligned the Lamin A/C profile generated in LCLs to the
240 Lamin B1 profile generated in Mutu I cells, we found that viral regions that associated with Lamin
241 B1 in Mutu I cells also associated with Lamin A/C in LCLs. Among the viral regions was the ~35
242 kb region, containing part of the coding region for EBNA2, and the TR region (**Figures 4A and**
243 **4B**). These results indicate that during latency nuclear lamins bind the EBV genome, but the
244 extent of such interaction changes between latency types. In Type I latency, Lamin B1 binds a
245 large portion of the EBV genome, while only few regions of the viral genome are associated with
246 either Lamin B1 or Lamin A/C in Type III latently infected cells. Moreover, our data indicated that
247 although most of the Lamin A/C binding occurs at EBV regions associated with Lamin B1, few
248 regions exist where Lamin A/C binds alone.. Overall, these results show that the EBV genome
249 interacts with nuclear lamins during latency, and that this property may underlie differential EBV
250 genomic subnuclear localization in different latency states.

251 **EBV regions associated with the nuclear lamina are enriched for the heterochromatin mark**
252 **H3K9me2.** Lamin A/C exists also in a nucleoplasmic form. Since the type of lamins associated
253 with the EBV genome changes between Type I and Type III latency, and also in type III latency
254 the genomic regions that bind Lamin A/C and Lamin B1 overlap only minimally, we speculated
255 that in Type III only a few EBV regions are localized at the nuclear lamina. To determine the
256 position of regions of the EBV genome at the nuclear lamina we assessed the presence across

257 the viral episome of the histone mark H3K9me3. The histone modification H3K9me2 is found at
258 the nuclear periphery of mammalian cell nuclei and enriched at genomic regions that are
259 associated with nuclear lamina [42, 58-61]. Thus, regions of heterochromatin that are enriched
260 for H3K9me2 are considered to be located at the nuclear periphery and associated with nuclear
261 lamina. First, we assessed the localization of H3K9me2 mark within the nuclear space in Mutu I
262 and LCLs cells by immunofluorescence microscopy (**Figure 5A**). In both cell lines, H3K9me2
263 staining localized at the nuclear rim. Merged images of H3K9me2 staining and Lamin B1staining
264 show that the two proteins colocalized, confirming that the H3K9me2 mark was enriched at
265 chromatin regions positioned at the nuclear periphery (**Figure 5A**). Next, we assessed the
266 H3K9me2 deposition across the EBV genome in latently infected cells. We reasoned that, if a
267 region was interacting with Lamin B1 or Lamin A/C and was enriched for the H3K9me2 mark,
268 then that region should be located at the nuclear periphery. We used ChIP-seq to assess
269 H3K9me2 levels across the EBV genome in Mutu I and LCLs (**Figure 5B**). Based on the peak-
270 calling analysis of ChIP-seq track for H3K9me2, we found that the H3K9me2 mark decorated
271 several chromatin regions of the EBV genome in Mutu I cells but only very few viral regions in
272 LCL cells (**Figure 5B**). In particular, we observed that in Type I latently infected Mutu cells
273 H3K9me2 decorated a ~ 50 kb of EBV genome that span the TR regions and the latent promoter
274 Qp and encompasses the EBV latent replication origin Ori P, the region encoding for the EBERs
275 and the promoter Cp, which is essential to support the Type III latency gene expression program
276 (**Figure 5B**). In Type III latently infected LCLs, H3K9me3 deposition was observed at very few
277 viral loci that mostly codes for lytic genes, including the region upstream the transcription start
278 site for the lytic transactivator gene BZLF1 (**Figure 5B**). Upon comparison of the binding profiles
279 of H3K9me2 and Lamin B1 across the EBV genome in Mutu I cells, we noticed that several
280 regions showed an overlap between H3K9me2 occupancy and Lamin B1 binding (**Supplemental**
281 **Figure 1**). Interesting Lamin B1 binding and H3K9me2 deposition overlapped and the TR regions
282 and the regions upstream the Qp promoter, which represent the boundaries of the large regions

283 of the EBV genome that is decorated with H3K9me2 in Type I latency (**Supplemental Figure 1**).
284 These results indicate that in Type I cells, a large portion of the EBV genome is localized at the
285 nuclear periphery. In LCLs, we next determined the overlap between Lamin A/C and H3K9me2
286 binding enrichment (**Figure 5C**). Regions enriched for both H3K9me2 and Lamin A/C occupancy
287 were identified, highlighting that only a few regions associated with Lamin A/C were also enriched
288 for H3K9me2 (**Figure 5C**) and indicating that certain viral genomic regions can be positioned at
289 the nuclear periphery. In LCLs, among the regions where Lamin A/C binding and H3K9me2
290 enrichment overlapped was a region around ~35bk and 40 kb of the viral genome, which contains
291 an *oriLyt*, part of the coding region for EBNA2 and the TR regions of EBV. Interestingly, these
292 were the same regions where Lamin A/C and Lamin B1 co-occupy the EBV genome in LCLs.
293 Overall, these results indicated that through nuclear lamina interactions, different EBV genomic
294 regions are positioned at the nuclear periphery in Type I and Type III latency.

295 **Lamin A/C is necessary to modulate the expression of EBV genes.** Interaction with the
296 nuclear lamina regulates gene expression, and changes in Lamin B1 and Lamin A/C occupancy
297 are linked to changes in transcription [62-71]. Since we observed changes in Lamin A/C
298 expression upon EBV infection and between type I and type III latently infected EBV+ B cells we
299 hypothesized that changes in Lamin A/C expression and occupancy across the viral genome
300 could contribute to regulating EBV gene expression during latency. To test this, we used
301 CRISPR/Cas9 gene editing to knock out Lamin A/C expression in LCLs (**Figure 6**). We used two
302 different single-guide RNAs (sgRNAs) that target distinct regions of the Lamin A/C gene to
303 generate two distinct Lamin A/C knockout LCL pools. Western blot analysis confirmed depletion
304 of Lamin A/C protein (**Figure 6A**). We next used immunofluorescence microscopy to determine
305 whether Lamin A/C knockout altered the structure of the nuclear lamina in LCLs (**Figure 6B**).
306 Staining for Lamin B1 was similar in WT and KO cells and localized to the nuclear rim (**Figure**
307 **6B)**. DAPI staining confirmed that Lamin KO had no effect on the overall shape of the nucleus or

308 the nuclear lamina. As expected, no Lamin A/C staining was seen in KO cells (**Figure 6B**). Next,
309 we tested whether the depletion of Lamin A/C affected EBV genome association with Lamin B1.
310 We assessed Lamin B1 occupancy at specific EBV genome regions in WT and KO cells by
311 quantitative ChIP (**Figure 6C**). Lamin B1 ChIP showed that, in the absence of Lamin A/C, Lamin
312 B1 occupancy was lost at the viral region around ~35 kb (EBNA2); however, at the TR region and
313 the Zp promoter Lamin B1 binding between the wildtype and the knockout was unchanged
314 (**Figure 6C**). Since we observed that in LCLs viral regions that associated with Lamin A/C were
315 also enriched for the heterochromatin mark H3K9me2 (**Figure 5B**), we used ChIP to assess the
316 effect of Lamin A/C absence on this mark (**Figure 6D**). The ChIP experiment showed that in Lamin
317 A/C KO cells, H3K9me2 enrichment was lost at the region ~35 kb of the EBV genome (EBNA2),
318 consistent with the loss of Lamin B1 in the same cells (**Figure 6D**). In contrast to Lamin B1
319 however, we observed that H3K9me2 enrichment was lost also at the EBV genomic TR region
320 and Z promoter (**Figure 6D**). These results demonstrated that Lamin A/C binding is important for
321 coordinating the binding of Lamin B1 at specific EBV genome regions and that Lamin A/C
322 occupancy is important for deposition of the H3K9me2 mark across the viral genome.

323 **KO of Lamin A/C alters the expression of EBV genes.** Interaction with the nuclear lamina is
324 linked to gene repression. In Lamin A/C KO cells, we observed changes in both Lamin B1
325 occupancy and H3K9me2 enrichment across the EBV genome. We asked whether the absence
326 of Lamin A/C could affect the expression of EBV genes. To address this question, we analyzed
327 the global gene expression of the viral genome in LCL KO vs WT cells (**Figure 7**). The changes
328 in viral gene expression observed in Lamin A/C KO cells are summarized by principal
329 component analysis (PCA) (**Figure 7A**). Principal component 1 separates samples by
330 presence of Lamin A/C, with the Wt samples and the KO samples diverging along the X-
331 axis. We next compared the changes in viral gene expression caused by Lamin A/C
332 knock-out. The RNA-seq data showed that in Lamin A/C KO cells, 27 viral transcripts were

333 differentially expressed ($p<0.05$) compared to WT cells (Figure 7B). This corresponds to a global
334 alteration in the expression of ~25% of all EBV genes in Lamin A/C KO LCLs. We found that 11
335 out the 27 viral genes were downregulated in KO cells, while the remaining 16 viral transcript
336 were up-regulated (Figure 7B). All the downregulated viral genes code for viral proteins that play
337 a role during EBV viral lytic replication including BFLF2. Interesting BFLF2 is a gene which codes
338 for a protein (the nuclear egress protein 1) that has been reported to interact with nuclear lamina
339 and to alter the nuclear membrane structure. Almost all of the up-regulated viral gene instead are
340 viral genes that are expressed during EBV type III latency, including the EBNA3s, the LMPs, the
341 EBERs, and EBNA2 (**Figure 7B**). The upregulation of EBNA2 is consistent with the observation
342 that in Lamin A/C KO cells the region encompassing the EBNA2 transcript lost Lamin B1 binding
343 and H3K9me2 deposition (**Figure 6B**). These results indicate that in Type III latency Lamin A/C
344 can control EBV gene expression and suggest a potential role of Lamin A/C in regulating the
345 switch between latent to lytic infection of EBV. Since that only at few loci of the EBV genome
346 Lamin A/C binding correlated with H3K9me2 deposition (Figure 5), we decided to assess whether,
347 perturbing H3K9me2 levels, could affect EBV gene expression in WT and Lamin A/C KO cells.
348 To do so we inhibited for 24 hours LCL WT and KO cells with a potent inhibitor of G9a, the histone
349 methyltransferases responsible for dimethylation of lysine 9 of the histone H3. We observed a
350 robust reduction of H3K9me2 levels in both WT and KO cells after 24 hours treatment with the
351 G9a inhibitors (**Figure 7C**). We next used RNA-seq to assess changes in EBV gene expression
352 after G9a inhibition in both WT and Lamin A/C KO LCL cells. The changes in viral gene
353 expression observed in Wt and KO cells after treatment with the G9a inhibitor are
354 summarized by principal component analysis (PCA) (**Figure 7A**). Principal component 2
355 separates well the LCL WT samples by treatment but not completely the Lamin A/C KO
356 samples (**Figure. 7A**). This is unsurprising considering that there are more EBV sites
357 associated with Lamin A/C than with H3K9me2 in Type III latency (Figure 5B). In fact,

358 when we assessed changes in the expression between treated and untreated cells in
359 Lamin KO cells we found only 4 viral genes (BTRF1, LMP1, BFRF3 and BNLF2b) with
360 significant changes in their expression. Instead, in LCL WT cells we found that inhibition
361 of G9a altered the expression of 12 viral genes (7 down-regulated and 5 up-regulated)
362 (**Figure 7D**). All the viral genes that were upregulated upon G9a inhibition are EBV genes
363 express in lytic reactivation, while all the repressed genes are latent genes, including
364 EBNA1, which is essential for the EBV maintenance in latently infected cells (**Figure 7B**).
365 These data suggest that in Type III latently infected cells H3K9me2 is an important histone
366 mark for the proper epigenetic silencing of the EBV lytic infection. Overall, our results
367 show that nuclear lamina is an important regulator of EBV viral gene expression during
368 latency.

369 **DISCUSSION**

370 EBV adopts alternative latency types in infected cells. We and others have previously
371 demonstrated that epigenetics plays an important role in regulating EBV gene expression during
372 latency [21, 22]. Our work demonstrated that both composition and structure of EBV chromatin
373 differ between latency types. An important epigenetic regulator of gene expression is the
374 interaction of the genome with nuclear lamina. Genomic regions that associated with nuclear
375 lamina and are positioned at the nuclear periphery are often poorly expressed and their chromatin
376 is strongly associated with repressive heterochromatin marks such as H3K9me2 [34-36]. To
377 further determine the contribution of epigenetic modifications on EBV latency we assessed the
378 role of nuclear lamina on EBV gene expression in latently infected cells. In our initially analysis,
379 we observed that EBV infection and viral latency can change the composition of nuclear lamina
380 (i.e. expression Lamin B1 and Lamin A/C) in B cells. We found that in addition to Lamin B1, EBV+
381 cell lines with type III latency and primary B cells infected with EBV express also Lamin A/C.

382 Recent work demonstrates that in immune cells, Lamin A/C is rapidly expressed upon antigen
383 activation[72]. In fact, we were able to phenocopy the EBV-induced Lamin A/C expression by
384 activating primary B cells with CD40 treatment. Our results with CD40L stimulation suggest that
385 the EBV CD40 mimic LMP1 may particularly be important for Lamin A/C upregulation.

386 The observed differences in nuclear lamina composition correlate with differential binding of
387 Lamin B1 and Lamin A/C across the viral genome between Type I and Type III latency. In Type I
388 EBV+ cells, we observed that Lamin B1 bind most of the viral genome. In Type III latency, Lamin
389 B1 is localized at nuclear periphery and transcriptionally repressed chromatin and heterochamatic
390 regions tend to localize at the nuclear periphery. Therefore, the increased Lamin B1 occupancy
391 we observed in Type I is in agreement with the increased transcriptionally silencing of viral gene
392 expression occurring in Type I gene expression program. We have previously reported that similar
393 differences exist in the DNA methylation levels and histone epigenetic marks across the EBV
394 gene between Type I and Type III latency [21, 73]. Thus, our results suggests that transcriptionally
395 silent EBV genomes tend to localize at the nuclear periphery.

396 In Type III latently infected B cells, Lamin A/C binding across the EBV genome did not necessarily
397 coincide with Lamin B1 occupancy. Instead, Lamin A/C and Lamin B1 co-occupy only a few EBV
398 genomic regions in LCLs. Differences exist between Lamin A and Lamin B1 with respect to their
399 function and sub-nuclear distribution. For example, while Lamin B1 is mostly positioned at the
400 nuclear membrane, Lamin A/C exists as a nucleoplasmic pool indicating that Lamin A/C is very
401 mobile inside the nuclear space. Based on this observation, we are tempted to speculate that in
402 Type III latency, regions of the EBV genome where Lamin B1 and Lamin A/C overlap are
403 positioned at the nuclear periphery, whereas regions bound by Lamin A/C alone are positioned
404 toward the nuclear center. These regions of EBV can be still repressed by Lamin A/C as
405 transcriptional silencing can occur without relocation of genomic regions to the nuclear envelope.

406 Our results suggest however that changes in nuclear lamina composition induced by EBV
407 infection contribute to the epigenetic regulation of the viral gene expression during latency.

408 Histone 3 lysine 9 dimethylation (H3K9me2) repressive marks were associated with Lamin B1
409 binding across the EBV genome and accumulated in the viral genome of Type I latent cells. This
410 is consistent with the work from the Van Steensel group which showed that, interaction of genomic
411 regions with the nuclear lamina depends on the H3K9me2 state within these regions [32]. Thus,
412 our data suggest that in Type I latency, viral regions localized at the nuclear periphery are
413 characterized by Lamin B1 binding and H2K9me2 deposition. Interesting, in Type III latency,
414 H3K9me2 deposition occurs only at viral genomic regions where Lamin B1 and Lamin A/C binding
415 colocalize, whereas regions bound by Lamin A/C alone had no H3K9me3 deposition. Our data
416 reveal that H2K9me2 is an important histone modification that participates in the epigenetic
417 regulation of EBV latency.

418 Based on our observations and the reported mobility of Lamin A/C within the nuclear space, we
419 are tempted to speculate that in Type I latently infected B cells, Lamin B1 positions the EBV
420 genome at the nuclear periphery, where silencing heterochromatin marks can then be deposited
421 across the viral genome. In Type III latently infected B cells, only few regions of the EBV episome
422 are positioned at the nuclear periphery, while other regions, through their association with Lamin
423 A/C, can shuttle between the nuclear periphery and the nuclear interior. In this model, Lamin A/C
424 binding alone is not sufficient to repress viral gene expression, but Lamin A/C is necessary for
425 the relocation of EBV genome at the nuclear periphery. Interestingly, recent studies from XXX
426 demonstrated that during adipocyte differentiation, Lamin A/C binds regions that relocate to the
427 nuclear periphery. Further studies are necessary to establish the exact mechanism of Lamin A/C
428 regulation of EBV episome, but our data suggest that a distinct role of lamin A and lamin B exists
429 in the regulation of viral gene expression in peripheral and the central regions of the nucleus in
430 the context of EBV latent infection.

431 Lamin A/C and H3K9me2 deposition are necessary to silence the transcription of EBV latent
432 genes. Our Lamin A/C KO cells show an increase in the expression of EBNA2 viral transcripts
433 and other latent EBV genes. Interestingly, in Type III cells Lamin A/C, Lamin B1, and H3K9me2
434 bind at the region of EBV coding for the EBNA2 specific exon. Binding of Lamin A/C may interfere
435 with the ability of Pol II to transcribe the EBNA2 transcript. Interestingly, pharmacological inhibition
436 of the histone methyltransferase G9a (responsible for H3K9me2 deposition) has a similar effect
437 as Lamin A/C depletion on EBV gene expression in Type III latency, suggesting that Lamin A/C
438 binding may repress EBV latent gene expression by tethering the EBV episome at the nuclear
439 periphery. This is consistent with a recent study showing that the inhibition of an H3K9
440 methyltransferase (G9a) lowered H3K9me2 levels at lamina associate domains and resulted in
441 lamina associated domain detachment from nuclear lamina[32]. These results indicate that
442 association with nuclear lamina represses EBV viral gene expression. Moreover, our results
443 suggest that G9a may be an important epigenetic regulator for EBV latency. Overall, our work
444 shows for the first time that interaction with nuclear lamina represents a novel epigenetic
445 mechanism that contributes to regulate EBV gene expression during latency.

446 Nuclear lamina plays a well-known anti-viral role in herpesvirus replication, including EBV, HSV1
447 and HSV2, and HCMV. During viral replication, the nuclear lamina represents a physical barrier
448 that prevents viral capsid egress. Elegant work from the Knipe group also reported the importance
449 of nuclear lamina in the formation of HSV-1 viral replication compartments [44, 45, 47, 49]. Our
450 data reveal an antiviral function during EBV latency, by contributing to the formation of an
451 epigenetic “barrier” across the viral genome that prevents viral gene expression. These findings
452 add a new branch to the existing model of how the host nuclear environment responds to viral
453 infection and may open a new direction in virus-host interaction research: the anti-viral role of
454 nuclear lamina in epigenetically repress viral gene expression.

455 Our work has some limitations. Although we observed binding of Lamin A/C in Type III latency to
456 the EBV genome, it is still possible that Lamin A/C may work as a repressor of latent gene
457 expression in cooperation with other cellular factors or transcription factors that can further help
458 to tether the EBV viral genome at the nuclear periphery. It is interesting to note, that a similar
459 model has been proposed for the regulation of HSV-1 lytic gene expression by Lamin A/C (PMID).
460 It will be of interest to identify the cellular factor(s) that synergize with nuclear lamina to position
461 EBV genome at the nuclear periphery. Our observed changes in nuclear lamina composition may
462 also affect the host gene expression, which we left unexplored in this current work. Although such
463 studies are beyond the scope of our work, the role of Lamin A/C on host gene expression may be
464 relevant as differentiating cells and cancer cells can change the composition of the nuclear lamina
465 (e.g., expression of Lamin A/C). In the next months, we are planning to explore this aspect of our
466 work.

467 In summary, our results, together with previous work from our group and others, reveal a novel
468 and unrecognized function of nuclear lamina in the host response against intrusion of viral DNA
469 into the nucleus by showing that Lamin B1 and Lamin A/C are important regulators of EBV gene
470 expression during latency. Our work adds an important branch to the existing model of how host
471 epigenetic factors regulate viral chromatin, and how the host and the viruses communicate to
472 regulate gene expression through modifying chromatin. Gaining a better insight into the nuclear
473 lamina/EBV interaction will reveal new important molecular steps that are necessary for cells to
474 control viral replication.

475

476 **MATERIALS AND METHODS**

477 **Cell culture and treatment**. Cell lines were maintained in a humidified atmosphere containing
478 5% CO_2 at 37°C. EBV positive cell lines were cultured in suspension in RPMI 1640 supplemented
479 with fetal bovine serum at a concentration of either 10% for type I latency (Mutu and Kem I) or
480 15% for type III latency (LCL, Kem III, and GM12878). All cell media were supplemented with 1%
481 penicillin-streptomycin. UNC0631 G9a/GPL inhibitor (Selleck Chemical) was dissolved in
482 dimethyl sulfoxide (DMSO) and diluted in the appropriate cell medium for treatment. Mutu I, LCL
483 and sg2 cells were treated with 1 μM UNC0631 for 24 h or as specified. The concentration of
484 UNC0631 used in experiments does not produce a cellular phenotype and does not induce DNA
485 damage.

486 **CRISPR Cas9 Mutagenesis**

487 B-cells were transduced with lentiviruses expressing sgRNAs, as previously described [74].
488 Briefly, lentiviruses were produced by transfection of 293T cells, which were plated in a 6-well
489 dish at a density of 600,000 cells per well in 2 mL DMEM supplemented with 10% fetal calf serum
490 24 hours before transfection. Transfection was done using the TransIT-LT1 Transfection Reagent
491 (Mirus). Two solutions were prepared for each well: a solution with 4 mL of LT1 diluted in 16 mL
492 of Opti-MEM (Corning) and incubated at room temperature for 5 min. The second solution
493 contained 150 ng pCMV-VSVG (Addgene 8454), 400 ng psPAX2 (Addgene 12260), and 500 ng
494 plentiguide puro expression vector (Addgene cat # 52963), in a final volume of 20 mL with Opti-
495 MEM. The two solutions were then mixed and incubated at room temperature for 30 min, added
496 dropwise to wells and gently mixed. Plates were returned to a 37C humidified chamber with 5%
497 CO2. The following day, media was exchanged to RPMI with 10% fetal calf serum. Virus
498 supernatant was harvested 48h post-transfection and filtered through a 0.4 uM sterile filter. Fresh
499 media was replenished on the 293T producer cell and a, second harvest, was done 72h post-

500 transfection and again sterile filtered. Virus supernatant was added to target cells at 48- and 72-
501 hours post-transfection. Target cell selection was begun 48 hours post-transduction by addition
502 of puromycin 3g/ml. sgRNA sequences used were as follows. Control:
503 ATTTCGCAGATCATCGACAT. LMNA: GCGCCGTCATGAGACCCGAC and
504 AGTTTAAGGAGCTGAAAGCG.

505 **B cell activation and B cells infection.**

506 Platelet-depleted venous blood, obtained from the Brigham and Women's Hospital bank, were
507 used for primary human B cell isolation, following institutional guidelines for discarded and de-
508 identified samples. CD19+ B-cells were isolated by negative selection as follows. RosetteSep
509 (Stem Cell Technologies, #15064) and EasySep negative isolation kits (Stem Cell Technologies,
510 #19054) were used to sequentially isolate B-cells, with the following modifications of the
511 manufacturer's protocols. For RosetteSep, 40 µL of antibody cocktail was added per mL of blood
512 and layered onto Lymphoprep density medium for centrifugation. For EasySep, 10 µL of antibody
513 cocktail was added per mL of B cells, followed by 15 µL of magnetic bead suspension per mL of
514 B cells. Following this negative selection, FACS for CD19 plasma membrane expression was
515 used to confirm B cell purity. The following reagents were used for B-cell stimulation: MEGA-
516 CD40L (Enzo Life Sciences Cat#ALX-522-110-C010, 50ng/mL), CpG (IDT,
517 TCGTCGTTTTGTCGTTTTGTCGTT, 1µM), αIgM (Sigma Cat#10759, 1mg/mL), IL-4 (R&D
518 Systems Cat#204-IL-050, 20ng/mL), αIgG (Agilent Cat#A042402-2). Cells were cultured in RPMI-
519 1640 (Invitrogen), supplemented with 10% standard FBS and penicillin-streptomycin. Cells were
520 cultured in a humidified incubator at 37°C and at 5% CO2.

521 **Western blot analysis.** Cell lysates were prepared in radioimmunoprecipitation assay (RIPA)
522 lysis buffer (50 mM Tris-HCl, pH 7.4, 150 mM NaCl, 0.25% deoxycholic acid, 1% NP-40, 1 mM
523 EDTA; Millipore) supplemented with 1× protease inhibitor cocktail (Thermo Scientific). Protein

524 extracts were obtained by centrifugation at 3,000 × *g* for 10 min at 4°C. Protein concentration was
525 measured using a bicinchoninic acid (BCA) protein assay (Pierce). Lysates were boiled with 2×
526 Laemmli sample buffer (Bio-Rad) containing 2.5% β-mercaptoethanol (Sigma-Aldrich). Proteins
527 were resolved by gel electrophoresis on a 4 to 20% polyacrylamide gradient Mini-Protean TGX
528 precast gel (Bio-Rad) and transferred to an Immobilon-P membrane (Millipore). Membranes were
529 blocked in 5% milk in PBS-T for 1 h at room temperature and incubated overnight at 4°C with
530 primary antibodies against Lamin AC (Active Motif 39287), Lamin B1 (Abcam ab16048), EBNA2
531 (Abcam ab90543), LMP1 (Abcam ab78113), and actin (Sigma-Aldrich A2066) as recommended
532 per the manufacturer. Membranes were washed, incubated for 1 h with the appropriate secondary
533 antibody, either goat anti-rabbit IgG-HRP (Jackson Immuno Research) or rabbit anti-mouse IgG-
534 HRP (Jackson Immuno Research). Membranes were then washed and detected by enhanced
535 chemiluminescence.

536 **Proteomic analysis.**

537 Samples were prepared for LC-MS/MS experiments are described previously[75]. Samples
538 were prepared for LC-MS/MS analysis as described above except samples were normalized to
539 total protein amount. A protein bicinchoninic acid assay was used on clarified lysate before
540 reduction and alkylation. Additionally, after labelling samples with TMT-11 reagents, samples
541 were normalized based on ratio check data to ensure a 1:1:1:1:1:1:1:1:1 total protein ratio was
542 observed as described previously[75]. For each BPRP fractionated sample, 12 of the 24 fractions
543 were selected for LC-MS/MS analysis to reduce redundant identifications. Each fraction was
544 analyzed on a Thermo Orbitrap Fusion Lumos with a Proxeon EASY-nLC 1200 system before
545 the source (Thermo Fisher Scientific, San Jose). The mass spectrometer was operated in a data-
546 dependent centroid mode for all SPS-MS3 methods. On-line chromatography was performed on
547 a 100μm inner diameter microcapillary column packed with 35cm of Accucore C18 resin was
548 used. Approximately 2μg of labelled peptides were loaded onto the column. Spectra were

549 acquired across a 90-minute LC gradient ranging from 6-25% acetonitrile in 0.125% formic acid.
550 For the 10-condition experiment, a real-time search method was employed in the instrument such
551 that SPS-MS3 scans would not trigger unless a successful Comet search result was obtained
552 from a preceding MS2 scan[76]. Spectra from all mass spectrometry experiments were
553 processed and searched with an in-house Sequest-based software pipeline as described
554 previously[75, 77, 78]. Raw data acquired on mass spectrometer instruments were converted into
555 an mzXML format before a Sequest search was executed against a human proteome database
556 (Uniprot Database ID: 9606, downloaded February 4, 2014). This database was concatenated
557 with common laboratory contaminants and a database comprised of all protein sequences
558 reversed. Ion tolerances for precursor and product ions were set to 50ppm and 0.9 Da
559 respectively. A variable mass difference of +15.99491 Da was assigned to methionine residues
560 to account for potential oxidation. Additionally, fixed modifications on cysteine (+57.02146 Da)
561 and lysine and the peptide N-terminus (+229.16293 Da) were assigned to account for protective
562 alkylation and TMT-11 labelling, respectively.

563 **RNA extraction and RNA-seq**

564 Total RNA for Lamin A/C knockout and G9a inhibition treatment experiment was isolated from
565 1.5 x 10^6 cells using using a PureLink RNA Mini Kit (ThermoFisher) according to the
566 manufacturer's protocol. RNA samples were submitted to the Wistar Institute genomics core
567 facility for initial analysis of RNA quality, with each sample having a RIN value greater than 8.5
568 (TapeStation, Agilent Technologies). Sequencing library preparation was then completed using
569 the QuantSeq 3'-mRNA kit (Lexogen) to generate Illumina-compatible sequencing libraries
570 according to the manufacturer's instructions. Single reads of 75 bp were obtained using a
571 NextSeq 500 sequencer. RNA-seq data was aligned using bowtie2 [79] against hg19 version of
572 the human genome and all unaligned reads were then aligned against NC_007605.1 version of
573 EBV genome and RSEM v1.2.12 software [80] was used to estimate raw read counts and RPKM

574 for EBV genes. DESeq2 [81] was used to estimate significance of differential expression between
575 groups pairs. Genes that passed nominal p<0.05 (FDR<20%) threshold were reported. The data
576 was submitted to GEO under accession number GSE181012

577 **Immunofluorescence assay.** For cell seeding sterile cover slips or slides can be used and
578 coated with adhesive material, Poly-L-Lysine (PLL). ~500 ul of 0.5 *10^6/ml cells resuspended in
579 media can be seeded on the coverslip and incubate overnight in a humidified atmosphere
580 containing 5% CO_2 at 37°C. Cells were fixed with 4% PFA and incubate at room temperature for
581 10 minutes. Cover slips washed for three times with Ca2+/Mg2+ free PBS. Then permeabilize in
582 PBS + 0.1% Triton X for 10 minutes at room temperature and then washed for three times with
583 Ca2+/Mg2+ free PBS. Coverslip were blocked in chi block (5% serum, 1%BSA in Ca2+/Mg2+
584 free PBS) for 1 hour at room temperature. Incubation with primary antibody diluted in chi block
585 [28]at 1:100 at room temperature for an hour. Wash with PBS + 0.1% Triton X for three times,
586 each wash 5 minutes. Incubation with secondary antibody, diluted 1:1000 in chi block and
587 incubated at room temperature for an hour. (This and the rest of the steps need to be done in the
588 dark). Wash with PBS + 0.1% Triton X for three times, each wash 5 minutes last wash without
589 tween. Mounting by adding a drop of pro Long Diamond antifade mountant with DAPI, let it mount
590 overnight and image the next day.

591 **ChIP-seq**. Chromatin immunoprecipitation with next-generation sequencing (ChIP-seq) was
592 performed as previously described [28] with minor changes. A total of 2.5×10^7 cells were cross-
593 linked with 1% formaldehyde for 10 min, and chromatin was sonicated with a Qsonica sonicator.
594 One-tenth of the sonicated chromatin was collected and used as input material, while the rest of
595 the chromatin was immunoprecipitated using 5 µg of Lamin AC antibody (Active Motif), 5 µg of
596 Lamin B1 antibody (Abcam), H3K9me2 antibody (Abcam ab6002), or 5 µg of normal rabbit IgG
597 (Cell Signaling) in LCLs and Mutu I. DNA fragments of ∼150 to 300 bp were visualized by agarose

598 gel purification. Immunoprecipitated DNA was ligated to adapter primers using the TruSeq ChIP
599 library preparation kit (Illumina) and then sequenced using the Illumina HiSeq 2500 platform
600 according to the manufacturer's recommendations (Illumina) at the Fox Chase Cancer Center
601 Sequencing Facility. For both LCL and Mutu I, ~15 ng of Lamin A/C, B1 and H3k9me2-
602 immunoprecipitated or input DNA was recovered from each biological replicate. Sequenced reads
603 were trimmed for quality and sequencing adapters using trimmomatic [82] then aligned to the EBV
604 genome using bowtie2 [79]. Aligned reads were prepared for visualization in IGV browser using
605 samtools [83] and BigWig tools [84]. Peaks were called using macs2 broad peaks and differential
606 peaks identified using macs2 bdgdiff [85]. Heatmaps and traces were made using deepTools [86]

607 **ChIP-qPCR.** ChIP assays were performed according to the Upstate Biotechnology, Inc.,
608 protocol as described previously, with minor modifications [28]. Briefly, cells were fixed in 1%
609 formaldehyde for 15 min, and DNA was sonicated using a Qsonica sonicator to generate 200- to
610 500-bp fragments. Chromatin was immunoprecipitated with antibodies to LaminB1 (abcam),
611 Lamin A/C (Active Motif) and H3K9me2 (abcam). Real-time PCR was performed with a master
612 mix containing 1× Maxima SYBR green, 0.25 μM primers, and 1/50 of the ChIP DNA per well.
613 Quantitative PCRs were carried out in triplicate using the ABI StepOnePlus PCR system. Data
614 were analyzed by the $\Delta\Delta C_T$ method (where C_T is threshold cycle) relative to DNA input and
615 normalized to the IgG control.

616 **qRT-PCR.** For quantitative reverse transcription-PCR (qRT-PCR), RNA was extracted from 2
617 × 10^6 cells using TRIzol (Thermo Fisher Scientific) according to the manufacturer's instructions.
618 SuperScript IV reverse transcriptase (Invitrogen) was used to generate randomly primed cDNA
619 from 1 μg of total RNA. A 50-ng cDNA sample was analyzed in triplicate by quantitative PCR
620 using the ABI StepOnePlus system. Data were analyzed by the $\Delta\Delta C_T$ method relative to
621 expression of 18S and normalized to controls.

622 **Histone Extraction.** Cell were harvest and wash twice using ice-cold PBS. Cell were
623 resuspended it in Triton Extraction Buffer (TEB: PBS containing 0.5% Triton X 100 (v/v), 2mM
624 phenylmethyl sulfonyl fluoride (PMSF), 0.02% (w/v) NaN3 at a cell density of 107 cells per ml.
625 Cell were lysed on ice for 10 minutes with gentle stirring, centrifugated at 2000 rpm for 10 minutes
626 at 4 C. The supernatant was removed and discarded. Cells washed in half the volume of TEB and
627 centrifuge at before. Pellets resuspend in 0.2N HCl at a cell density of 4x107 cells per ml. Acid
628 extraction of histones over night at 4 C. Next day samples were centrifuge at 2000 rpm for 10
629 minutes at 4 C. The supernatant moved to a new clean tube and determinate the protein content
630 by Bradford assay.

631 **Statistical analysis.** All experiments presented were conducted at least in triplicate to ensure
632 reproducibility of results. The Prism statistical software package (GraphPad) was used to identify
633 statistically significant differences between experimental conditions and control samples, using
634 Student's *t* test as indicated in the figure legends.

635 **AKNWOLEDGMENTS**

636 Research reported in this publication was supported by the National Institute of Allergy
637 and Infectious Diseases of the National Institutes of Health under Award Number
638 R01AI130209 to IT and R01AI164709 and CA228700 to BG, a Burroughs Wellcome
639 Career Award in Medical Sciences, and a Lymphoma Research Foundation Fellowship
640 to RG.

641

642 **REFERENCES**

643 1. 1. G. de-The NED, A. Geser, et al. . Sero-epidemiology of the Epstein-Barr virus:
644 preliminary analysis of an international study – a review. IARC Sci Publ 1975:pp. 3-16
645 2. Ohga S NA, Takada H, et al Immunological aspects of Epstein-Barr virus infection. . Crit
646 Rev Oncol Hematol 2002. doi: 10.1016/S1040-8428(02)00112-9. PubMed Central PMCID:
647 PMC12467961.
648 3. Chang CM, Yu KJ, Mbulaiteye SM, Hildesheim A, Bhatia K. The extent of genetic diversity
649 of Epstein-Barr virus and its geographic and disease patterns: a need for reappraisal. Virus Res.
650 2009;143(2):209-21. Epub 2009/07/15. doi: 10.1016/j.virusres.2009.07.005. PubMed PMID:
651 19596032; PubMed Central PMCID: PMCPMC2731007.
652 4. Cohen JI, Fauci AS, Varmus H, Nabel GJ. Epstein-Barr virus: an important vaccine target
653 for cancer prevention. Sci Transl Med. 2011;3(107):107fs7. Epub 2011/11/04. doi:
654 10.1126/scitranslmed.3002878. PubMed PMID: 22049067; PubMed Central PMCID:
655 PMCPMC3501269.
656 5. Sarwari NM, Khoury JD, Hernandez CM. Chronic Epstein Barr virus infection leading to
657 classical Hodgkin lymphoma. BMC Hematol. 2016;16:19. Epub 2016/07/21. doi: 10.1186/s12878-
658 016-0059-3. PubMed PMID: 27437106; PubMed Central PMCID: PMCPMC4950766.
659 6. Khan G, Hashim MJ. Global burden of deaths from Epstein-Barr virus attributable
660 malignancies 1990-2010. Infect Agent Cancer. 2014;9(1):38. Epub 2014/12/05. doi:
661 10.1186/1750-9378-9-38. PubMed PMID: 25473414; PubMed Central PMCID:
662 PMCPMC4253616.
663 7. Hsu JL, Glaser SL. Epstein-barr virus-associated malignancies: epidemiologic patterns
664 and etiologic implications. Crit Rev Oncol Hematol. 2000;34(1):27-53. Epub 2000/04/27. doi:
665 10.1016/s1040-8428(00)00046-9. PubMed PMID: 10781747.

666 8. Taylor GS, Long HM, Brooks JM, Rickinson AB, Hislop AD. The immunology of Epstein-
667 Barr virus-induced disease. Annu Rev Immunol. 2015;33:787-821. Epub 2015/02/24. doi:
668 10.1146/annurev-immunol-032414-112326. PubMed PMID: 25706097.
669 9. Rickinson AB. Co-infections, inflammation and oncogenesis: future directions for EBV
670 research. Semin Cancer Biol. 2014;26:99-115. Epub 2014/04/23. doi:
671 10.1016/j.semcancer.2014.04.004. PubMed PMID: 24751797.
672 10. Hatton OL, Harris-Arnold A, Schaffert S, Krams SM, Martinez OM. The interplay between
673 Epstein-Barr virus and B lymphocytes: implications for infection, immunity, and disease. Immunol
674 Res. 2014;58(2-3):268-76. Epub 2014/03/13. doi: 10.1007/s12026-014-8496-1. PubMed PMID:
675 24619311; PubMed Central PMCID: PMCPMC4199828.
676 11. Thorley-Lawson DA. EBV Persistence--Introducing the Virus. Curr Top Microbiol Immunol.
677 2015;390(Pt 1):151-209. Epub 2015/10/02. doi: 10.1007/978-3-319-22822-8_8. PubMed PMID:
678 26424647; PubMed Central PMCID: PMCPMC5125397.
679 12. Thorley-Lawson DA. Epstein-Barr virus: exploiting the immune system. Nat Rev Immunol.
680 2001;1(1):75-82. Epub 2002/03/22. doi: 10.1038/35095584. PubMed PMID: 11905817.
681 13. Rowe M, Lear AL, Croom-Carter D, Davies AH, Rickinson AB. Three pathways of Epstein-
682 Barr virus gene activation from EBNA1-positive latency in B lymphocytes. J Virol. 1992;66(1):122-
683 31. Epub 1992/01/01. doi: 10.1128/JVI.66.1.122-131.1992. PubMed PMID: 1309242; PubMed
684 Central PMCID: PMCPMC238267.
685 14. De Leo A, Calderon A, Lieberman PM. Control of Viral Latency by Episome Maintenance
686 Proteins. Trends Microbiol. 2020;28(2):150-62. Epub 2019/10/19. doi: 10.1016/j.tim.2019.09.002.
687 PubMed PMID: 31624007; PubMed Central PMCID: PMCPMC6980450.
688 15. Chiu YF, Sugden B. Plasmid Partitioning by Human Tumor Viruses. J Virol. 2018;92(9).
689 Epub 2018/02/23. doi: 10.1128/JVI.02170-17. PubMed PMID: 29467315; PubMed Central
690 PMCID: PMCPMC5899212.

691 16. Lieberman PM. Virology. Epstein-Barr virus turns 50. Science. 2014;343(6177):1323-5.
692 Epub 2014/03/22. doi: 10.1126/science.1252786. PubMed PMID: 24653027; PubMed Central
693 PMCID: PMCPMC4581426.
694 17. Sugden B. Epstein-Barr virus: the path from association to causality for a ubiquitous
695 human pathogen. PLoS Biol. 2014;12(9):e1001939. Epub 2014/09/03. doi:
696 10.1371/journal.pbio.1001939. PubMed PMID: 25180782; PubMed Central PMCID:
697 PMCPMC4151957.
698 18. Thorley-Lawson DA, Allday MJ. The curious case of the tumour virus: 50 years of Burkitt's
699 lymphoma. Nat Rev Microbiol. 2008;6(12):913-24. Epub 2008/11/15. doi: 10.1038/nrmicro2015.
700 PubMed PMID: 19008891.
701 19. Takacs M, Banati F, Koroknai A, Segesdi J, Salamon D, Wolf H, et al. Epigenetic
702 regulation of latent Epstein-Barr virus promoters. Biochim Biophys Acta. 2010;1799(3-4):228-35.
703 Epub 2009/10/27. doi: 10.1016/j.bbagrm.2009.10.005. PubMed PMID: 19853674.
704 20. Tempera I, Lieberman PM. Chromatin organization of gammaherpesvirus latent genomes.
705 Biochim Biophys Acta. 2010;1799(3-4):236-45. Epub 2009/10/27. doi:
706 10.1016/j.bbagrm.2009.10.004. PubMed PMID: 19853673; PubMed Central PMCID:
707 PMCPMC2839031.
708 21. Tempera I, Lieberman PM. Epigenetic regulation of EBV persistence and oncogenesis.
709 Semin Cancer Biol. 2014;26:22-9. Epub 2014/01/29. doi: 10.1016/j.semcancer.2014.01.003.
710 PubMed PMID: 24468737; PubMed Central PMCID: PMCPMC4048758.
711 22. Arvey A, Tempera I, Lieberman PM. Interpreting the Epstein-Barr Virus (EBV) epigenome
712 using high-throughput data. Viruses. 2013;5(4):1042-54. Epub 2013/04/04. doi:
713 10.3390/v5041042. PubMed PMID: 23549386; PubMed Central PMCID: PMCPMC3705264.
714 23. Zhang Y, Jiang C, Trudeau SJ, Narita Y, Zhao B, Teng M, et al. Histone Loaders CAF1
715 and HIRA Restrict Epstein-Barr Virus B-Cell Lytic Reactivation. mBio. 2020;11(5). Epub

716 2020/10/29. doi: 10.1128/mBio.01063-20. PubMed PMID: 33109754; PubMed Central PMCID:
717 PMCPMC7593962.
718 24. Barski A, Cuddapah S, Cui K, Roh TY, Schones DE, Wang Z, et al. High-resolution
719 profiling of histone methylations in the human genome. Cell. 2007;129(4):823-37. Epub
720 2007/05/22. doi: 10.1016/j.cell.2007.05.009. PubMed PMID: 17512414.
721 25. Dyson PJ, Farrell PJ. Chromatin structure of Epstein-Barr virus. J Gen Virol. 1985;66 (Pt
722 9):1931-40. Epub 1985/09/01. doi: 10.1099/0022-1317-66-9-1931. PubMed PMID: 2993484.
723 26. Tempera I, Klichinsky M, Lieberman PM. EBV latency types adopt alternative chromatin
724 conformations. PLoS Pathog. 2011;7(7):e1002180. Epub 2011/08/11. doi:
725 10.1371/journal.ppat.1002180. PubMed PMID: 21829357; PubMed Central PMCID:
726 PMCPMC3145795.
727 27. Arvey A, Tempera I, Tsai K, Chen HS, Tikhmyanova N, Klichinsky M, et al. An atlas of the
728 Epstein-Barr virus transcriptome and epigenome reveals host-virus regulatory interactions. Cell
729 Host Microbe. 2012;12(2):233-45. Epub 2012/08/21. doi: 10.1016/j.chom.2012.06.008. PubMed
730 PMID: 22901543; PubMed Central PMCID: PMCPMC3424516.
731 28. Lupey-Green LN, Caruso LB, Madzo J, Martin KA, Tan Y, Hulse M, et al. PARP1 Stabilizes
732 CTCF Binding and Chromatin Structure To Maintain Epstein-Barr Virus Latency Type. J Virol.
733 2018;92(18). Epub 2018/07/07. doi: 10.1128/JVI.00755-18. PubMed PMID: 29976663; PubMed
734 Central PMCID: PMCPMC6146685.
735 29. Collas P, Lund EG, Oldenburg AR. Closing the (nuclear) envelope on the genome: How
736 nuclear lamins interact with promoters and modulate gene expression. 2013;36(1):75 -- 83. doi:
737 10.1002/bies.201300138. PubMed PMID: Collas:2013ip.
738 30. Pickersgill H, Kalverda B, de Wit E, Talhout W, Fornerod M, van Steensel B.
739 Characterization of the Drosophila melanogaster genome at the nuclear lamina. Nat Genet.
740 2006;38(9):1005-14. Epub 2006/08/01. doi: 10.1038/ng1852. PubMed PMID: 16878134.

741 31. Burke B, Stewart CL. The nuclear lamins: flexibility in function. Nature Reviews Molecular
742 Cell Biology. 2012;14(1):13 -- 24. doi: 10.1038/nrm3488. PubMed PMID: Burke:2012kr.
743 32. Kind J, Pagie L, Ortabozkoyun H, Boyle S, Vries SSd, Janssen H, et al. Single-cell
744 dynamics of genome-nuclear lamina interactions. Cell. 2013;153(1):178 -- 92. doi:
745 10.1016/j.cell.2013.02.028. PubMed PMID: Kind:2013gg.
746 33. Ragoczy T, Telling A, Scalzo D, Kooperberg C, Groudine M. Functional redundancy in the
747 nuclear compartmentalization of the late-replicating genome. Nucleus. 2014;5(6):626-35. Epub
748 2014/12/11. doi: 10.4161/19491034.2014.990863. PubMed PMID: 25493640; PubMed Central
749 PMCID: PMCPMC4615584.
750 34. Peric-Hupkes D, van Steensel B. Role of the nuclear lamina in genome organization and
751 gene expression. Cold Spring Harb Symp Quant Biol. 2010;75:517-24. Epub 2011/01/07. doi:
752 10.1101/sqb.2010.75.014. PubMed PMID: 21209388.
753 35. Lund E, Oldenburg AR, Delbarre E, Freberg CT, Duband-Goulet I, Eskeland R, et al.
754 Lamin A/C-promoter interactions specify chromatin state-dependent transcription outcomes.
755 Genome Research. 2013;23(10):1580 -- 9. doi: 10.1101/gr.159400.113. PubMed PMID:
756 Lund:2013fr.
757 36. Dechat T, Pfleghaar K, Sengupta K, Shimi T, Shumaker DK, Solimando L, et al. Nuclear
758 lamins: major factors in the structural organization and function of the nucleus and chromatin.
759 Genes \& Development. 2008;22(7):832 -- 53. doi: 10.1101/gad.1652708. PubMed PMID:
760 Dechat:2008ea.
761 37. van Steensel B, Belmont AS. Lamina-Associated Domains: Links with Chromosome
762 Architecture, Heterochromatin, and Gene Repression. Cell. 2017;169(5):780-91. Epub
763 2017/05/20. doi: 10.1016/j.cell.2017.04.022. PubMed PMID: 28525751; PubMed Central PMCID:
764 PMCPMC5532494.

765 38. Verstraeten VL, Broers JL, Ramaekers FC, van Steensel MA. The nuclear envelope, a
766 key structure in cellular integrity and gene expression. Curr Med Chem. 2007;14(11):1231-48.
767 Epub 2007/05/17. doi: 10.2174/092986707780598032. PubMed PMID: 17504143.
768 39. Osmanagic-Myers S, Dechat T, Foisner R. Lamins at the crossroads of mechanosignaling.
769 Genes Dev. 2015;29(3):225-37. Epub 2015/02/04. doi: 10.1101/gad.255968.114. PubMed PMID:
770 25644599; PubMed Central PMCID: PMCPMC4318140.
771 40. Prokocimer M, Davidovich M, Nissim-Rafinia M, Wiesel-Motiuk N, Bar DZ, Barkan R, et
772 al. Nuclear lamins: key regulators of nuclear structure and activities. J Cell Mol Med.
773 2009;13(6):1059-85. Epub 2009/02/13. doi: 10.1111/j.1582-4934.2008.00676.x. PubMed PMID:
774 19210577; PubMed Central PMCID: PMCPMC4496104.
775 41. Worman HJ, Lazaridis I, Georgatos SD. Nuclear lamina heterogeneity in mammalian cells.
776 Differential expression of the major lamins and variations in lamin B phosphorylation. J Biol Chem.
777 1988;263(24):12135-41. Epub 1988/08/25. PubMed PMID: 3403563.
778 42. Hutchison CJ, Worman HJ. A-type lamins: guardians of the soma? Nat Cell Biol.
779 2004;6(11):1062-7. Epub 2004/11/02. doi: 10.1038/ncb1104-1062. PubMed PMID: 15517000.
780 43. Hutchison CJ, Bridger JM, Cox LS, Kill IR. Weaving a pattern from disparate threads:
781 lamin function in nuclear assembly and DNA replication. J Cell Sci. 1994;107 (Pt 12):3259-69.
782 Epub 1994/12/01. PubMed PMID: 7706384.
783 44. de Noronha CM, Sherman MP, Lin HW, Cavrois MV, Moir RD, Goldman RD, et al.
784 Dynamic disruptions in nuclear envelope architecture and integrity induced by HIV-1 Vpr. Science.
785 2001;294(5544):1105-8. Epub 2001/11/03. doi: 10.1126/science.1063957. PubMed PMID:
786 11691994.
787 45. Gonnella R, Farina A, Santarelli R, Raffa S, Feederle R, Bei R, et al. Characterization and
788 intracellular localization of the Epstein-Barr virus protein BFLF2: interactions with BFRF1 and with
789 the nuclear lamina. J Virol. 2005;79(6):3713-27. Epub 2005/02/26. doi: 10.1128/JVI.79.6.3713-
790 3727.2005. PubMed PMID: 15731265; PubMed Central PMCID: PMCPMC1075684.

791 46. Farina A, Santarelli R, Bloise R, Gonnella R, Granato M, Bei R, et al. KSHV ORF67
792 encoded lytic protein localizes on the nuclear membrane and alters emerin distribution. Virus Res.
793 2013;175(2):143-50. Epub 2013/04/30. doi: 10.1016/j.virusres.2013.04.001. PubMed PMID:
794 23623980.
795 47. Scott ES, O'Hare P. Fate of the inner nuclear membrane protein lamin B receptor and
796 nuclear lamins in herpes simplex virus type 1 infection. J Virol. 2001;75(18):8818-30. Epub
797 2001/08/17. doi: 10.1128/jvi.75.18.8818-8830.2001. PubMed PMID: 11507226; PubMed Central
798 PMCID: PMCPMC115126.
799 48. Muranyi W, Haas J, Wagner M, Krohne G, Koszinowski UH. Cytomegalovirus recruitment
800 of cellular kinases to dissolve the nuclear lamina. Science. 2002;297(5582):854-7. Epub
801 2002/08/06. doi: 10.1126/science.1071506. PubMed PMID: 12161659.
802 49. Mettenleiter TC, Klupp BG, Granzow H. Herpesvirus assembly: a tale of two membranes.
803 Curr Opin Microbiol. 2006;9(4):423-9. Epub 2006/07/04. doi: 10.1016/j.mib.2006.06.013. PubMed
804 PMID: 16814597.
805 50. Lee CP, Huang YH, Lin SF, Chang Y, Chang YH, Takada K, et al. Epstein-Barr virus
806 BGLF4 kinase induces disassembly of the nuclear lamina to facilitate virion production. J Virol.
807 2008;82(23):11913-26. Epub 2008/09/26. doi: 10.1128/JVI.01100-08. PubMed PMID: 18815303;
808 PubMed Central PMCID: PMCPMC2583647.
809 51. Wang C, Li D, Zhang L, Jiang S, Liang J, Narita Y, et al. RNA Sequencing Analyses of
810 Gene Expression during Epstein-Barr Virus Infection of Primary B Lymphocytes. J Virol.
811 2019;93(13). Epub 2019/04/26. doi: 10.1128/JVI.00226-19. PubMed PMID: 31019051; PubMed
812 Central PMCID: PMCPMC6580941.
813 52. Wang LW, Shen H, Nobre L, Ersing I, Paulo JA, Trudeau S, et al. Epstein-Barr-Virus-
814 Induced One-Carbon Metabolism Drives B Cell Transformation. Cell Metab. 2019;30(3):539-55
815 e11. Epub 2019/07/02. doi: 10.1016/j.cmet.2019.06.003. PubMed PMID: 31257153; PubMed
816 Central PMCID: PMCPMC6720460.

817 53. Price AM, Messinger JE, Luftig MA. c-Myc Represses Transcription of Epstein-Barr Virus
818 Latent Membrane Protein 1 Early after Primary B Cell Infection. J Virol. 2018;92(2). Epub
819 2017/11/10. doi: 10.1128/JVI.01178-17. PubMed PMID: 29118124; PubMed Central PMCID:
820 PMCPMC5752943.
821 54. Price AM, Tourigny JP, Forte E, Salinas RE, Dave SS, Luftig MA. Analysis of Epstein-Barr
822 virus-regulated host gene expression changes through primary B-cell outgrowth reveals delayed
823 kinetics of latent membrane protein 1-mediated NF-kappaB activation. J Virol.
824 2012;86(20):11096-106. Epub 2012/08/03. doi: 10.1128/JVI.01069-12. PubMed PMID:
825 22855490; PubMed Central PMCID: PMCPMC3457162.
826 55. Wang LW, Jiang S, Gewurz BE. Epstein-Barr Virus LMP1-Mediated Oncogenicity. J Virol.
827 2017;91(21). Epub 2017/08/25. doi: 10.1128/JVI.01718-16. PubMed PMID: 28835489; PubMed
828 Central PMCID: PMCPMC5640852.
829 56. Kieser A, Sterz KR. The Latent Membrane Protein 1 (LMP1). Curr Top Microbiol Immunol.
830 2015;391:119-49. Epub 2015/10/03. doi: 10.1007/978-3-319-22834-1_4. PubMed PMID:
831 26428373.
832 57. Tempera I, Wiedmer A, Dheekollu J, Lieberman PM. CTCF prevents the epigenetic drift
833 of EBV latency promoter Qp. PLoS Pathog. 2010;6(8):e1001048. Epub 2010/08/24. doi:
834 10.1371/journal.ppat.1001048. PubMed PMID: 20730088; PubMed Central PMCID:
835 PMCPMC2921154.
836 58. Poleshko A, Smith CL, Nguyen SC, Sivaramakrishnan P, Wong KG, Murray JI, et al.
837 H3K9me2 orchestrates inheritance of spatial positioning of peripheral heterochromatin through
838 mitosis. Elife. 2019;8. Epub 2019/10/02. doi: 10.7554/eLife.49278. PubMed PMID: 31573510;
839 PubMed Central PMCID: PMCPMC6795522.
840 59. Poleshko A, Mansfield KM, Burlingame CC, Andrake MD, Shah NR, Katz RA. The human
841 protein PRR14 tethers heterochromatin to the nuclear lamina during interphase and mitotic exit.

842 Cell Rep. 2013;5(2):292-301. Epub 2013/11/12. doi: 10.1016/j.celrep.2013.09.024. PubMed
843 PMID: 24209742; PubMed Central PMCID: PMCPMC3867587.
844 60. Holla S, Dhakshnamoorthy J, Folco HD, Balachandran V, Xiao H, Sun LL, et al. Positioning
845 Heterochromatin at the Nuclear Periphery Suppresses Histone Turnover to Promote Epigenetic
846 Inheritance. Cell. 2020;180(1):150-64 e15. Epub 2019/12/31. doi: 10.1016/j.cell.2019.12.004.
847 PubMed PMID: 31883795; PubMed Central PMCID: PMCPMC7102895.
848 61. Ho CY, Lammerding J. Lamins at a glance. J Cell Sci. 2012;125(Pt 9):2087-93. Epub
849 2012/06/07. doi: 10.1242/jcs.087288. PubMed PMID: 22669459; PubMed Central PMCID:
850 PMCPMC3367936.
851 62. Amendola M, van Steensel B. Mechanisms and dynamics of nuclear lamina-genome
852 interactions. Curr Opin Cell Biol. 2014;28:61-8. Epub 2014/04/04. doi: 10.1016/j.ceb.2014.03.003.
853 PubMed PMID: 24694724.
854 63. Malhas AN, Vaux DJ. Transcription factor sequestration by nuclear envelope components.
855 Cell Cycle. 2009;8(7):959-60. Epub 2009/03/17. doi: 10.4161/cc.8.7.8092. PubMed PMID:
856 19287201.
857 64. Dechat T, Pfleghaar K, Sengupta K, Shimi T, Shumaker DK, Solimando L, et al. Nuclear
858 lamins: major factors in the structural organization and function of the nucleus and chromatin.
859 Genes Dev. 2008;22(7):832-53. Epub 2008/04/03. doi: 10.1101/gad.1652708. PubMed PMID:
860 18381888; PubMed Central PMCID: PMCPMC2732390.
861 65. Collas P, Lund EG, Oldenburg AR. Closing the (nuclear) envelope on the genome: how
862 nuclear lamins interact with promoters and modulate gene expression. Bioessays. 2014;36(1):75-
863 83. Epub 2013/11/26. doi: 10.1002/bies.201300138. PubMed PMID: 24272858.
864 66. Burke B, Stewart CL. The nuclear lamins: flexibility in function. Nat Rev Mol Cell Biol.
865 2013;14(1):13-24. Epub 2012/12/06. doi: 10.1038/nrm3488. PubMed PMID: 23212477.
866 67. Shah PP, Donahue G, Otte GL, Capell BC, Nelson DM, Cao K, et al. Lamin B1 depletion
867 in senescent cells triggers large-scale changes in gene expression and the chromatin landscape.

868 Genes Dev. 2013;27(16):1787-99. Epub 2013/08/13. doi: 10.1101/gad.223834.113. PubMed
869 PMID: 23934658; PubMed Central PMCID: PMCPMC3759695.
870 68. Lund E, Oldenburg AR, Delbarre E, Freberg CT, Duband-Goulet I, Eskeland R, et al.
871 Lamin A/C-promoter interactions specify chromatin state-dependent transcription outcomes.
872 Genome Res. 2013;23(10):1580-9. Epub 2013/07/19. doi: 10.1101/gr.159400.113. PubMed
873 PMID: 23861385; PubMed Central PMCID: PMCPMC3787256.
874 69. Guelen L, Pagie L, Brasset E, Meuleman W, Faza MB, Talhout W, et al. Domain
875 organization of human chromosomes revealed by mapping of nuclear lamina interactions. Nature.
876 2008;453(7197):948-51. Epub 2008/05/09. doi: 10.1038/nature06947. PubMed PMID: 18463634.
877 70. Mattout-Drubezki A, Gruenbaum Y. Dynamic interactions of nuclear lamina proteins with
878 chromatin and transcriptional machinery. Cell Mol Life Sci. 2003;60(10):2053-63. Epub
879 2003/11/18. doi: 10.1007/s00018-003-3038-3. PubMed PMID: 14618255.
880 71. Kind J, Pagie L, Ortabozkoyun H, Boyle S, de Vries SS, Janssen H, et al. Single-cell
881 dynamics of genome-nuclear lamina interactions. Cell. 2013;153(1):178-92. Epub 2013/03/26.
882 doi: 10.1016/j.cell.2013.02.028. PubMed PMID: 23523135.
883 72. Contu F, Rangel-Pozzo A, Trokajlo P, Wark L, Klewes L, Johnson NA, et al. Distinct 3D
884 Structural Patterns of Lamin A/C Expression in Hodgkin and Reed-Sternberg Cells. Cancers
885 (Basel). 2018;10(9). Epub 2018/08/29. doi: 10.3390/cancers10090286. PubMed PMID:
886 30149530; PubMed Central PMCID: PMCPMC6162537.
887 73. Guo R, Zhang Y, Teng M, Jiang C, Schineller M, Zhao B, et al. DNA methylation enzymes
888 and PRC1 restrict B-cell Epstein-Barr virus oncoprotein expression. Nat Microbiol.
889 2020;5(8):1051-63. Epub 2020/05/20. doi: 10.1038/s41564-020-0724-y. PubMed PMID:
890 32424339; PubMed Central PMCID: PMCPMC7462085.
891 74. Ma Y, Walsh MJ, Bernhardt K, Ashbaugh CW, Trudeau SJ, Ashbaugh IY, et al.
892 CRISPR/Cas9 Screens Reveal Epstein-Barr Virus-Transformed B Cell Host Dependency

893 Factors. Cell Host Microbe. 2017;21(5):580-91 e7. Epub 2017/05/12. doi:
894 10.1016/j.chom.2017.04.005. PubMed PMID: 28494239.
895 75. Navarrete-Perea J, Yu Q, Gygi SP, Paulo JA. Streamlined Tandem Mass Tag (SL-TMT)
896 Protocol: An Efficient Strategy for Quantitative (Phospho)proteome Profiling Using Tandem Mass
897 Tag-Synchronous Precursor Selection-MS3. J Proteome Res. 2018;17(6):2226-36. Epub
898 2018/05/08. doi: 10.1021/acs.jproteome.8b00217. PubMed PMID: 29734811; PubMed Central
899 PMCID: PMCPMC5994137.
900 76. Erickson BK, Mintseris J, Schweppe DK, Navarrete-Perea J, Erickson AR, Nusinow DP,
901 et al. Active Instrument Engagement Combined with a Real-Time Database Search for Improved
902 Performance of Sample Multiplexing Workflows. J Proteome Res. 2019;18(3):1299-306. Epub
903 2019/01/20. doi: 10.1021/acs.jproteome.8b00899. PubMed PMID: 30658528; PubMed Central
904 PMCID: PMCPMC7081948.
905 77. Paulo JA, O'Connell JD, Gygi SP. A Triple Knockout (TKO) Proteomics Standard for
906 Diagnosing Ion Interference in Isobaric Labeling Experiments. J Am Soc Mass Spectrom.
907 2016;27(10):1620-5. Epub 2016/07/13. doi: 10.1007/s13361-016-1434-9. PubMed PMID:
908 27400695; PubMed Central PMCID: PMCPMC5018445.
909 78. Huttlin EL, Jedrychowski MP, Elias JE, Goswami T, Rad R, Beausoleil SA, et al. A tissue-
910 specific atlas of mouse protein phosphorylation and expression. Cell. 2010;143(7):1174-89. Epub
911 2010/12/25. doi: 10.1016/j.cell.2010.12.001. PubMed PMID: 21183079; PubMed Central PMCID:
912 PMCPMC3035969.
913 79. Langmead B, Salzberg SL. Fast gapped-read alignment with Bowtie 2. Nat Methods.
914 2012;9(4):357-9. Epub 2012/03/06. doi: 10.1038/nmeth.1923. PubMed PMID: 22388286;
915 PubMed Central PMCID: PMCPMC3322381.
916 80. Li B, Dewey CN. RSEM: accurate transcript quantification from RNA-Seq data with or
917 without a reference genome. BMC Bioinformatics. 2011;12:323. Epub 2011/08/06. doi:

918 10.1186/1471-2105-12-323. PubMed PMID: 21816040; PubMed Central PMCID:
919 PMCPMC3163565.
920 81. Love MI, Huber W, Anders S. Moderated estimation of fold change and dispersion for
921 RNA-seq data with DESeq2. Genome Biol. 2014;15(12):550. Epub 2014/12/18. doi:
922 10.1186/s13059-014-0550-8. PubMed PMID: 25516281; PubMed Central PMCID:
923 PMCPMC4302049.
924 82. Bolger AM, Lohse M, Usadel B. Trimmomatic: a flexible trimmer for Illumina sequence
925 data. Bioinformatics. 2014;30(15):2114-20. Epub 2014/04/04. doi:
926 10.1093/bioinformatics/btu170. PubMed PMID: 24695404; PubMed Central PMCID:
927 PMCPMC4103590.
928 83. Li H, Handsaker B, Wysoker A, Fennell T, Ruan J, Homer N, et al. The Sequence
929 Alignment/Map format and SAMtools. Bioinformatics. 2009;25(16):2078-9. Epub 2009/06/10. doi:
930 10.1093/bioinformatics/btp352. PubMed PMID: 19505943; PubMed Central PMCID:
931 PMCPMC2723002.
932 84. Kent WJ, Zweig AS, Barber G, Hinrichs AS, Karolchik D. BigWig and BigBed: enabling
933 browsing of large distributed datasets. Bioinformatics. 2010;26(17):2204-7. Epub 2010/07/20. doi:
934 10.1093/bioinformatics/btq351. PubMed PMID: 20639541; PubMed Central PMCID:
935 PMCPMC2922891.
936 85. Zhang Y, Liu T, Meyer CA, Eeckhoute J, Johnson DS, Bernstein BE, et al. Model-based
937 analysis of ChIP-Seq (MACS). Genome Biol. 2008;9(9):R137. Epub 2008/09/19. doi: 10.1186/gb-
938 2008-9-9-r137. PubMed PMID: 18798982; PubMed Central PMCID: PMCPMC2592715.
939 86. Ramirez F, Ryan DP, Gruning B, Bhardwaj V, Kilpert F, Richter AS, et al. deepTools2: a
940 next generation web server for deep-sequencing data analysis. Nucleic Acids Res.
941 2016;44(W1):W160-5. Epub 2016/04/16. doi: 10.1093/nar/gkw257. PubMed PMID: 27079975;
942 PubMed Central PMCID: PMCPMC498787

943 **FIGURE LEGENDS**

944 **Figure 1: Type I and Type III EBV+ cells express different components of nuclear**
945 **lamina**. **A)** Western blot for key EBV proteins (EBNA2, LMP1) and nuclear lamina components
946 (Lamin B1 and A/C) in EBV negative cell lines (B cells, Akata) and EBV+ positive cell lines that
947 express the type I (Mutu I) or the type III latency program (Mutu III, Mutu-LCL, B95.8-LCK,
948 GM12878). Actin was used as a loading control. Images are representative of at least three
949 independent experiments. **B)** Confocal microscopy images of EBV+ cells Mutu I and LCL stained
950 with DAPI or anti-Lamin B1 or anti-Lamin A/C antibodies. Both methods show that Lamin A/C is
951 differentially expressed, depending on the presence of EBV and its latency state. **C)** Higher
952 magnification of the boxed areas in B to better show the colocalization of the lamin proteins at the
953 nuclear periphery. **D)** Confocal microscopy images of single LCLs, demonstrating that the two
954 lamins do not completely overlap at the nuclear periphery and that Lamin B is located more
955 peripherally than Lamin A/C.

956 **Figure 2: EBV infection induces Lamin A/C RNA and protein expression. A)** Confocal
957 microscopy images of B cells, from healthy donors, before and after infection with EBV. After 35
958 days, when the EBV infection is established, cells start to express Lamin A/C. **B)** RNA-seq
959 analysis of Lamin A/C expression in primary B cells from human donors. The graph shows the
960 number of reads at different timepoints after EBV infection. **C)** Whole cell proteomic data showing
961 Lamin A/C induction at the indicated timepoints following infection with EBV in primary human B
962 cell. Data is from 3 biological replicates, representing 12 human donors.

963 **Figure 3: Activation of B cells by CD40 induces Lamin A/C expression. A)** Confocal
964 microscopy images of B cells from human donors in the resting and activated states with different
965 ligands (IL4, CD40 and CpG). Cells are stained with DAPI, or anti-Lamin B1 or anti-Lamin A/C
966 antibodies. The magnified images at the right show that Lamin A/C staining increased after

967 activation. **B)** RNA-Seq analysis showing expression levels of Lamin A/C, quantified by number
968 of reads, in B cells 24 hours after stimulation with the indicated ligands. The two bars for each
969 ligand indicate two different experiments done in parallel. C) Lamin A/C protein expression
970 samples are the same used in the RNA-Seq analysis in panel B.

971 **Figure 4: The EBV genome interacts with the nuclear lamins. A)** ChIP-seq data for Lamin
972 B1 and Lamin A/C in EBV+ B cells adopting type I (Mutu I) or type III (LCLs) latency, mapped to
973 the wild-type EBV genome. The image shows the ChIP-Seq profile for each antibody and each
974 cell used and the localization of the peak on the EBV genome indicated with small rectangles on
975 the bottom of the ChIP-Seq track. Note that the switch from type I to type III latency is
976 accompanied by a change in the lamin B1 binding profile. **B)** Zoom in of regions, to show that in
977 type I cells, Lamin B1 associates with the repressed Cp and LMP1 promoters on the EBV genome,
978 whereas in type III cells, Lamin A/C binding is enriched whereas Lamin B1 one is depleted at sites
979 of active transcription on the EBV genome.

980 **Figure 5: Heterochromatin mark H3K9me2 and nuclear lamin association in EBV**
981 **regions**. **A)** ChIP-seq analysis of H3K9me2 occupancy across the EBV genome, in EBV+ B cells
982 adopting type I (Mutu I) or type III (LCLs) latency, mapped to the wild-type EBV genome. The
983 rectangles below the ChIP-Seq tracks indicate where the bindings occur and, based on the
984 intensity of the color, if binding is strong or weak. H3K9me2 occupancy across the viral genome
985 differs between type I and type III EBV+ cells; H3K9me2 binds to fewer locations in type III cells
986 and the binding is stronger. **B)** Comparison of ChIP-Seq peaks locations for H3K9me2 and Lamin
987 A/C in LCLs. The red boxes indicate where the binding site for the two antibodies are the same.
988 These regions are localized at the EBNA2, BZLF2, BKRF4 and 3, RPMS1 and LMP2/1 promoters.
989 Note that nearly every H3K9me2 peak colocalizes with, or is near, a Lamin A/C peak. Data are
990 expressed as %input. N=3, Mean ± SD**. C)** Confocal microscopy images of Lamin B1 and

991 H3K9Me2 in type I (Mutu I) and type III (LCL) cells. Type III cell lines display the H3K9me2 mark
992 not only at the nuclear periphery but also in other parts of the nucleus.

993 **Figure 6: Lamin A/C knockdown reduces H3K9me2 and Lamin B1 binding at the EBV**
994 **EBNA2 promoter. A)** Confocal images of GM12878 cell lines in which two different guide RNAs,
995 Sg1 and Sg2, were used to knock down Lamin A/C. **B)**. Western blot for Lamin A/C or Lamin B1
996 in the same cell lines as in A. Actin was used as loading control. **C)** ChIP-qPCR results comparing
997 the binding, in control and Lamin A/C knockdown (Sg2) cells, of Lamin B1 or H3K9me2 at the
998 indicated EBV-relevant promoters. Data are calculated as %input. The promoter that experiences
999 the greatest change in Lamin B1 and H3K9m32 binding upon Lamin A/C knockdown is EBNA2.

1000 **Figure 7: The effect of Lamin A/C knockout and G9a inhibition on EBV gene expression**
1001 **profiles. A)** Principal Component Analysis of the RNA-Seq data performed on GM12878 control
1002 (WT.unt.1,2,3) GM12878 Lamin A/C knockout (KO.Unt.1,2) cells, and GM12878 WT and KO
1003 treated with G9a inhibitor (WTtrt.1,2,3 and KO.trt.1,2). The principal components 1 and 2 were
1004 chosen to better represent the samples clustering. **B)** Heat map showing genes that change
1005 significantly ($P<0.05$) between control and Lamin KO cell lines; differences were calculated using
1006 p-values. Note the presence of EBNAs and LMP1 family members. **C)** Western blot for nuclear
1007 lamina components (Lamin B1 and A/C) and histone mark H3K9me2 in both GM128787 control
1008 and Lamin A/C knockout treated with or without G9a inhibitor (-, +). Actin and H3 were used as
1009 loading control for respectively proteins and histone mark. Images are representative of at least
1010 three independent experiments. After the treatment with G9a we noticed a reduction in H3K9me2
1011 levels in both Gm12787 control and Lamin A/C knockout cell lines. **D)** Heat map of genes that
1012 significantly change expression upon inhibition with G9a in LCL WT cells compared to controls.

1013 **Supplemental Figure 1 Heterochromatin mark H3K9me2 differences in binding between**
1014 **Type I and Type III.** ChIP-seq analysis of H3K9me2 occupancy and Lamin B1 binding across the

1015 EBV genome, in EBV+ B cells adopting type I latency, Mutu I, mapped to the wild-type EBV
1016 genome. The rectangles below the ChIP-Seq tracks indicate binding regions identified by peak
1017 calling analysis, where the bindings occur and, based on the intensity of the color, if binding is
1018 strong or weak.

1019 **Supplemental Figure 2. IgG ChIP-qPCR.** ChIP-qPCR results comparing the binding, in
1020 control and Lamin A/C knockdown (Sg2) cells, of IgG at the indicated EBV-relevant promoters.
1021 Data are calculated as %input. N=3, Mean ± SD

1022

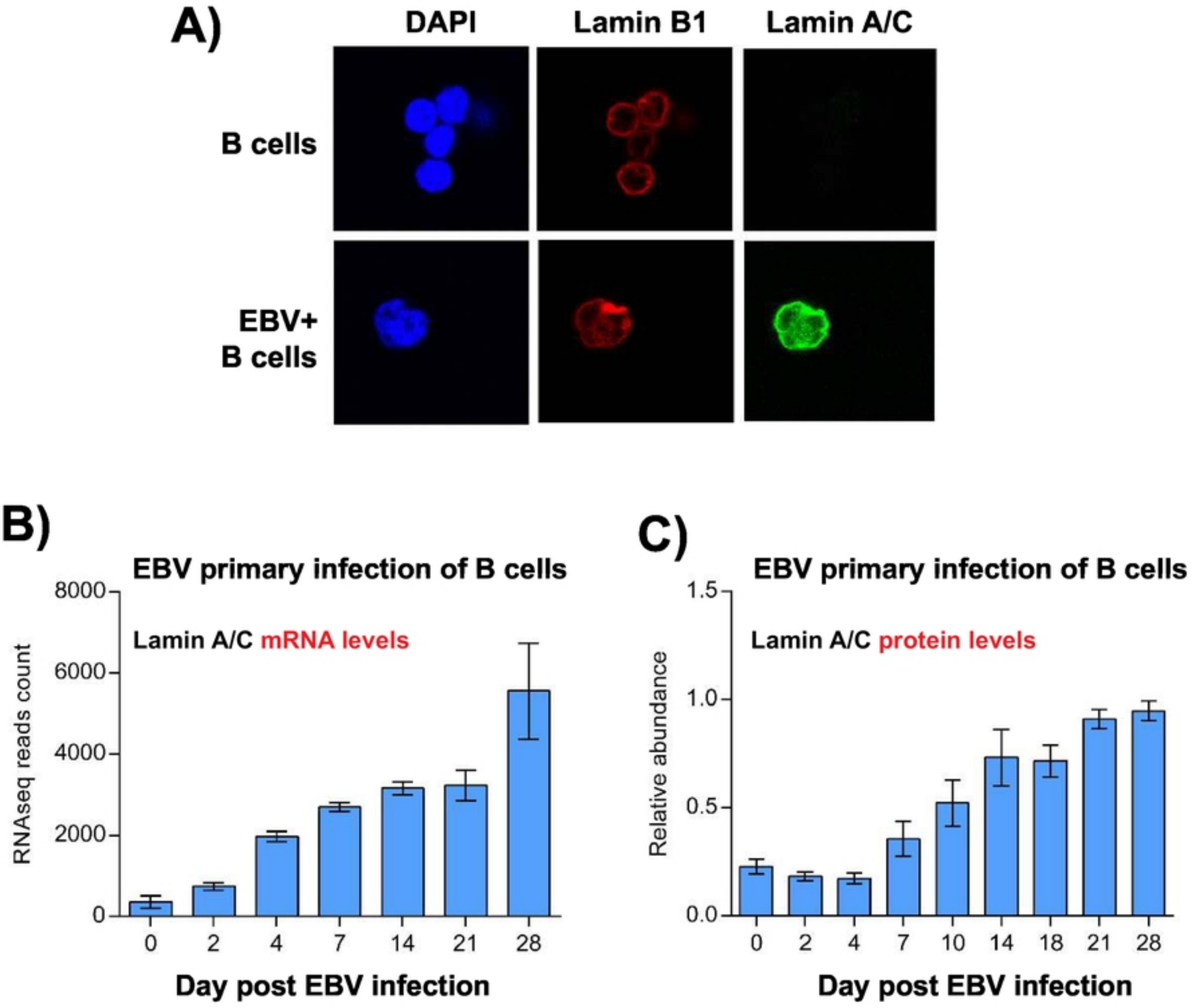
A)
DAPI
Lamin B1
Lamin A/C
B cells
EBV+
B cells
B)
EBV primary infection of B cells
Lamin A/C mRNA levels
RNAseq reads count
8000
6000
4000
2000
0
0
2
4
7
14
21
28
Day post EBV infection
C)
EBV primary infection of B cells
Lamin A/C protein levels
Relative abundance
1.5
1.0
0.5
0.0
0
2
4
7
10
14
18
21
28
Day post EBV infection

Figure 2

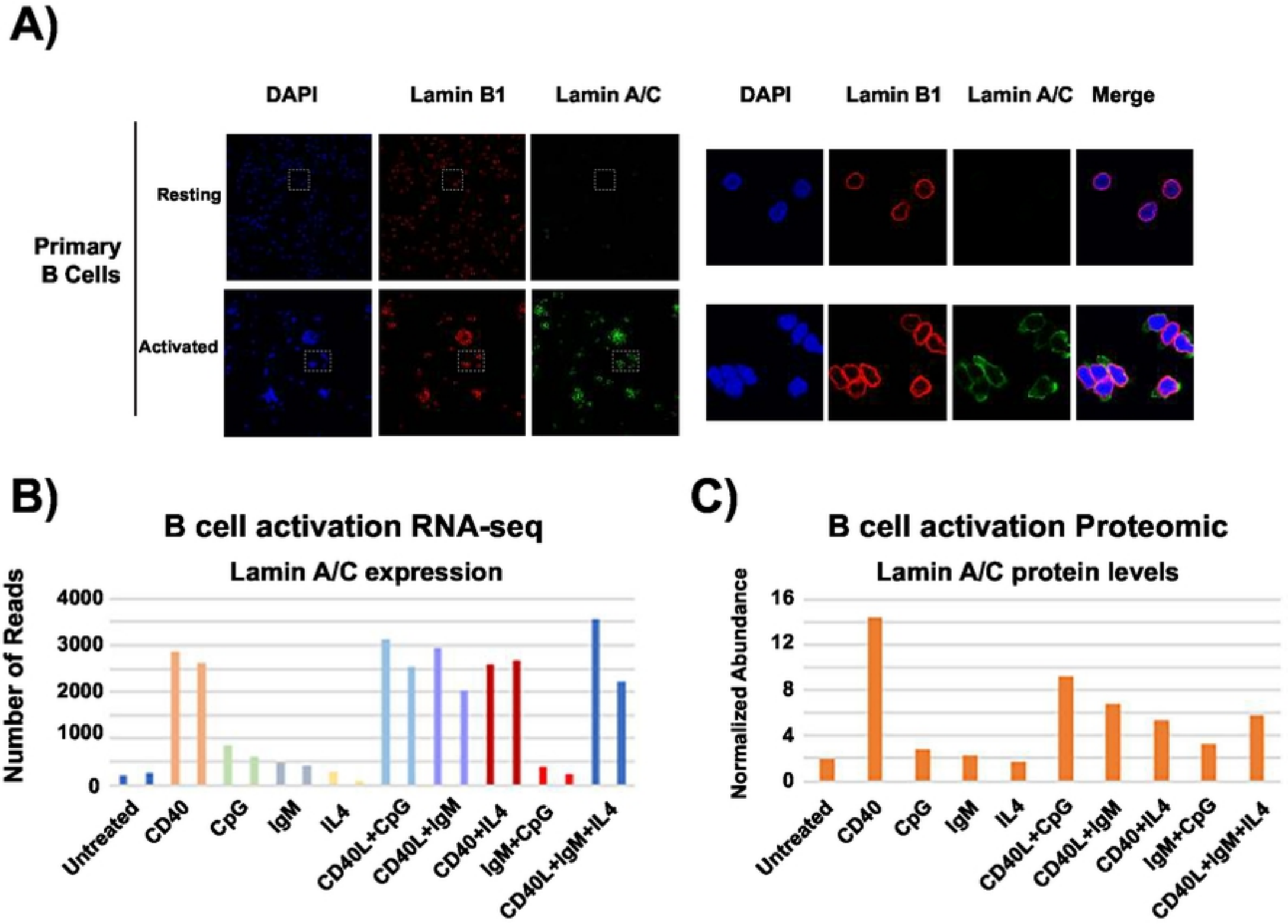
A)
DAPI
Lamin B1
Lamin A/C
DAPI
Lamin B1
Lamin A/C
Merge
Primary B Cells
Resting
Activated
B)
B cell activation RNA-seq
Lamin A/C expression
Number of Reads
4000
3000
2000
1000
0
Untreated
CD40
CpG
IgM
IL4
CD40L+CpG
CD40L+IgM
CD40+IL4
IgM+CpG
CD40L+IgM+IL4
C)
B cell activation Proteomic
Lamin A/C protein levels
Normalized Abundance
16
12
8
4
0
Untreated
CD40
CpG
IgM
IL4
CD40L+CpG
CD40L+IgM
CD40+IL4
IgM+CpG
CD40L+IgM+IL4

Figure 3

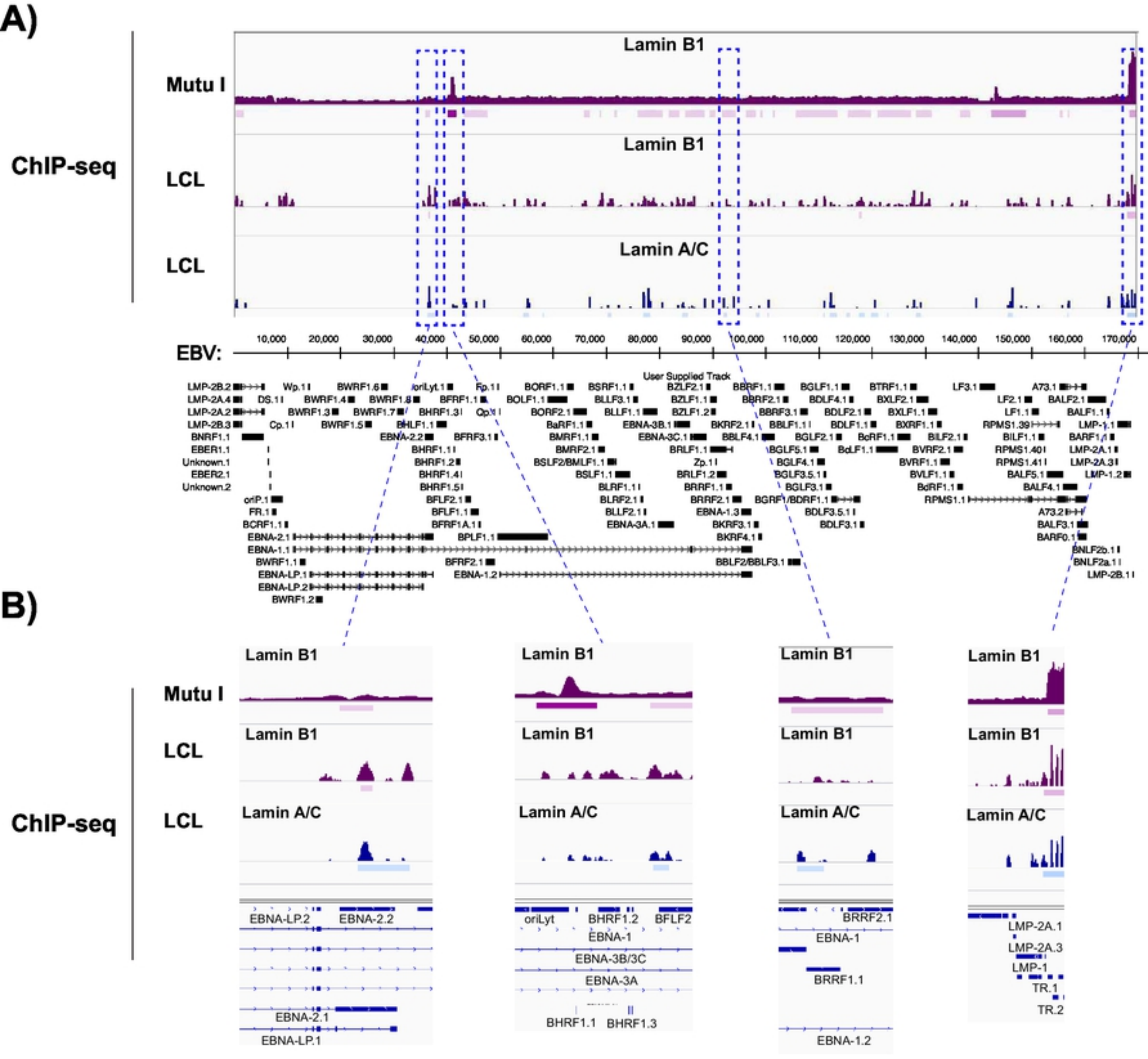
A)
ChIP-seq
Mutu I
LCL
LCL
Lamin B1
Lamin B1
Lamin A/C
EBV:
10,000
20,000
30,000
40,000
50,000
60,000
70,000
80,000
90,000
100,000
110,000
120,000
130,000
140,000
150,000
160,000
170,000
User Supplied Track
B)
ChIP-seq
Mutu I
LCL
LCL
Lamin B1
Lamin A/C
EBNA-LP.2
EBNA-2.2
EBNA-2.1
EBNA-LP.1
oriLyt
BHRF1.2
BFLF2
EBNA-1
EBNA-3B/3C
EBNA-3A
BHRF1.1
BHRF1.3
BRRF2.1
EBNA-1
BRRF1.1
EBNA-1.2
LMP-2A.1
LMP-2A.3
LMP-1
TR.1
TR.2

Figure 4

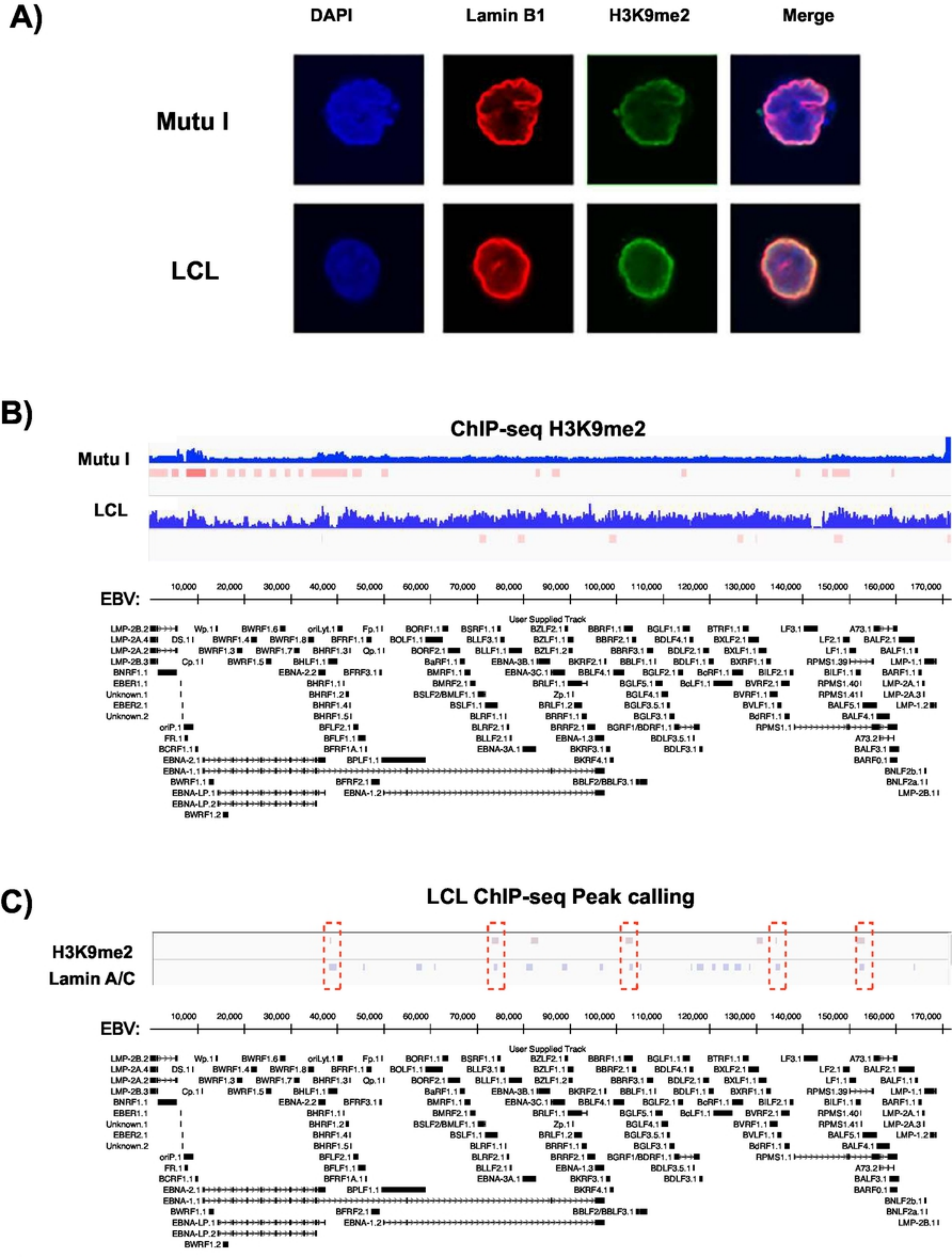
A)
DAPI
Lamin B1
H3K9me2
Merge
Mutu I
LCL
B)
ChIP-seq H3K9me2
Mutu I
LCL
EBV:
10,000
20,000
30,000
40,000
50,000
60,000
70,000
80,000
90,000
100,000
110,000
120,000
130,000
140,000
150,000
160,000
170,000
User Supplied Track
C)
LCL ChIP-seq Peak calling
H3K9me2
Lamin A/C
EBV:

Figure 5

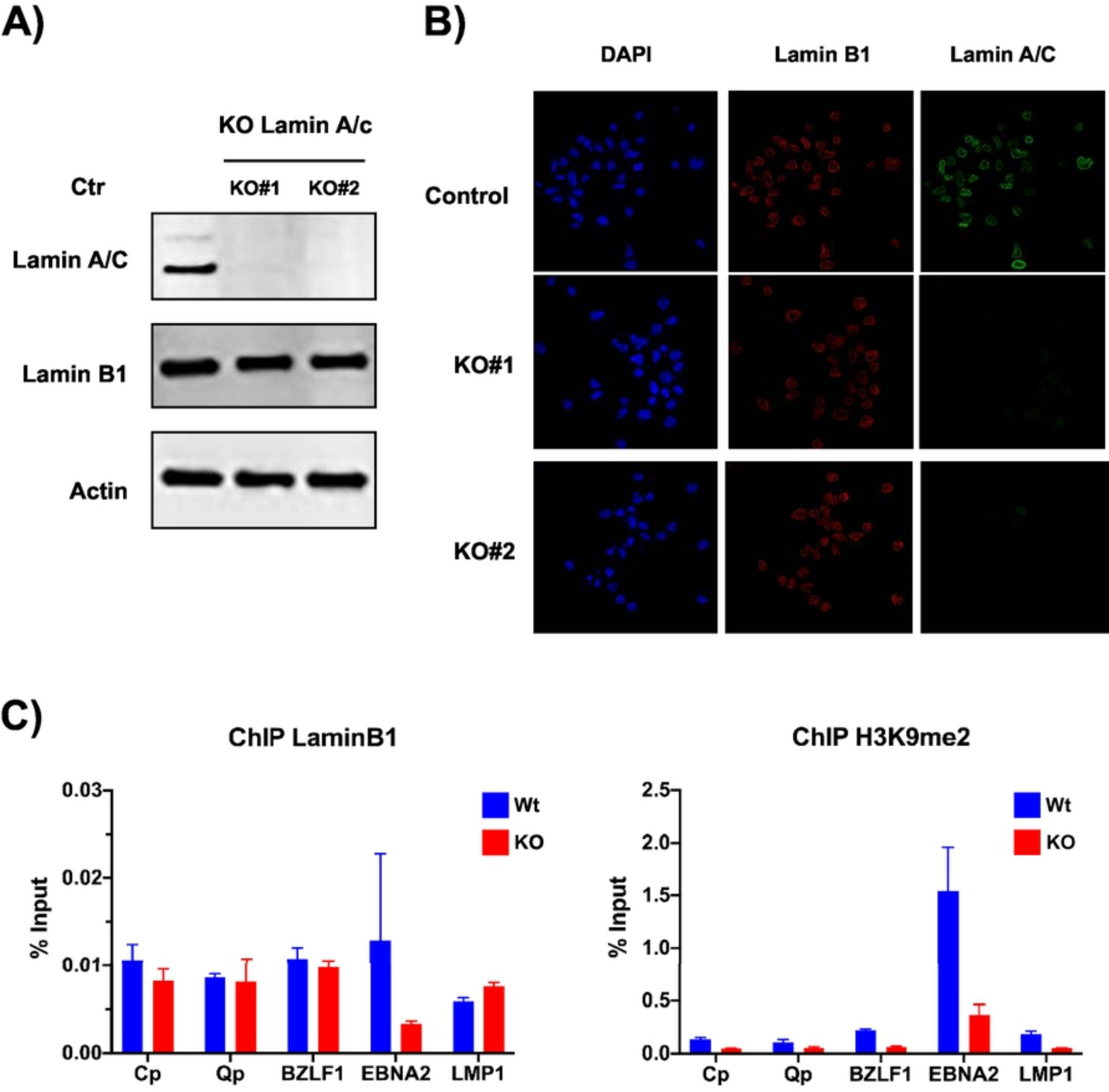
A)
KO Lamin A/c
Ctr
KO#1
KO#2
Lamin A/C
Lamin B1
Actin
B)
DAPI
Lamin B1
Lamin A/C
Control
KO#1
KO#2
C)
ChIP LaminB1
% Input
0.03
0.02
0.01
0.00
Wt
KO
Cp
Qp
BZLF1
EBNA2
LMP1
ChIP H3K9me2
% Input
2.5
2.0
1.5
1.0
0.5
0.0
Wt
KO
Cp
Qp
BZLF1
EBNA2
LMP1

Figure 6

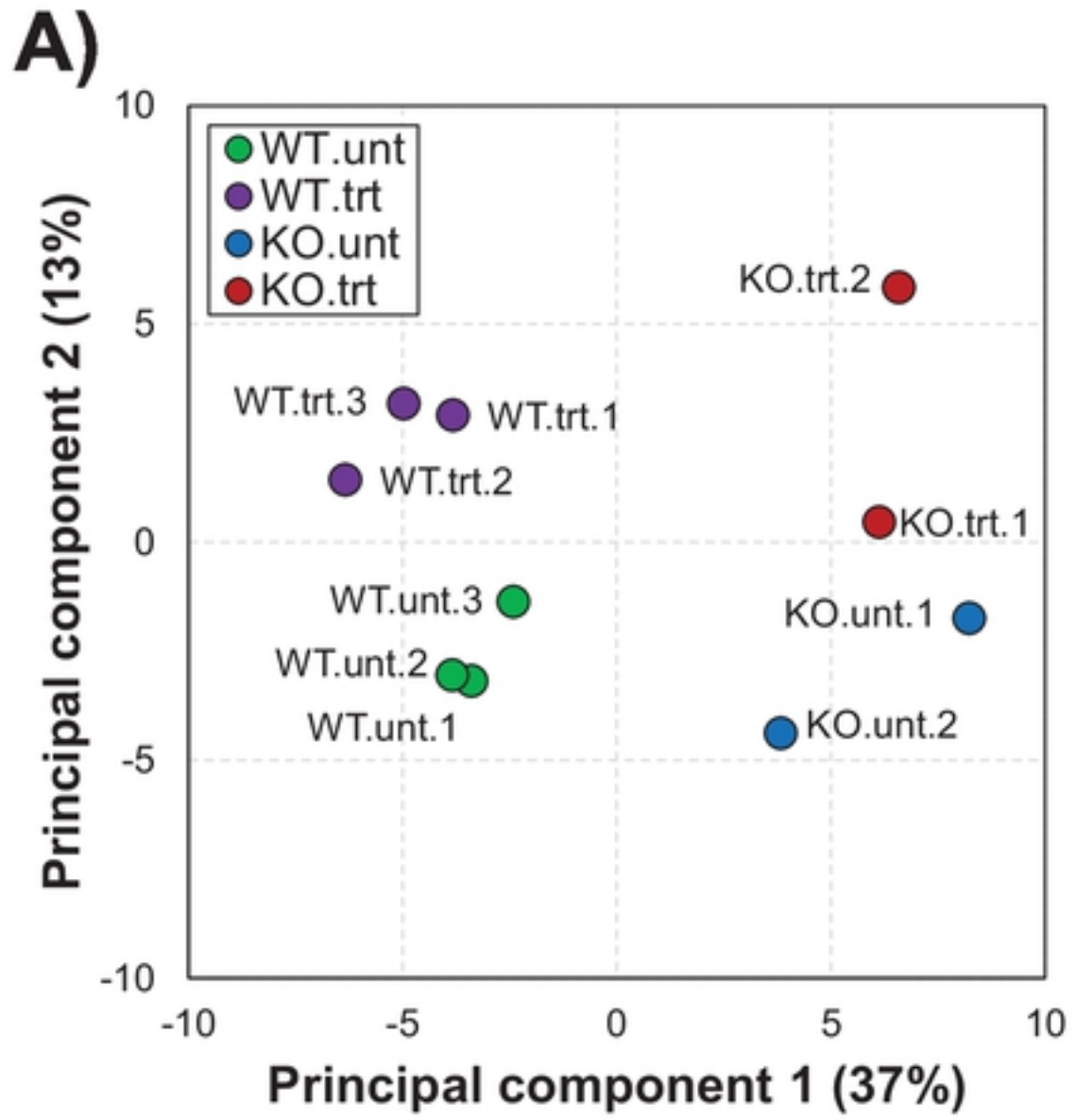
A)
WT.unt
WT.trt
KO.unt
KO.trt
KO.trt.2
WT.trt.3
WT.trt.1
WT.trt.2
KO.trt.1
WT.unt.3
KO.unt.1
WT.unt.2
WT.unt.1
KO.unt.2
Principal component 2 (13%)
Principal component 1 (37%)
10
5
0
-5
-10
-10
-5
0
5
10

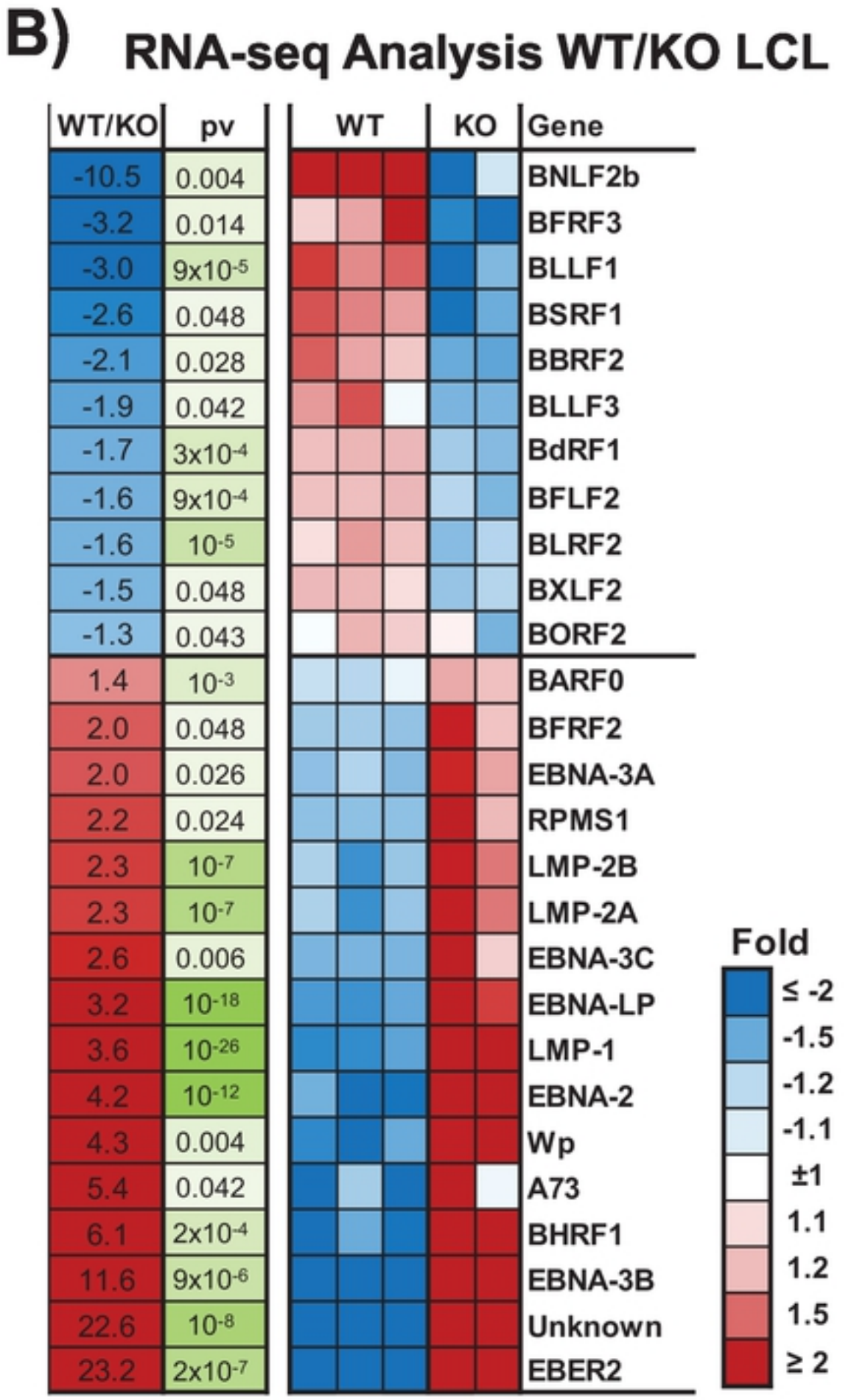
B)
RNA-seq Analysis WT/KO LCL
WT/KO
pv
WT
KO
Gene
-10.5 0.004 BNLF2b
-3.2 0.014 BFRF3
-3.0 9x10-5 BLLF1
-2.6 0.048 BSRF1
-2.1 0.028 BBRF2
-1.9 0.042 BLLF3
-1.7 3x10-4 BdRF1
-1.6 9x10-4 BFLF2
-1.6 10-5 BLRF2
-1.5 0.048 BXLF2
-1.3 0.043 BORF2
1.4 10-3 BARF0
2.0 0.048 BFRF2
2.0 0.026 EBNA-3A
2.2 0.024 RPMS1
2.3 10-7 LMP-2B
2.3 10-7 LMP-2A
2.6 0.006 EBNA-3C
3.2 10-18 EBNA-LP
3.6 10-26 LMP-1
4.2 10-12 EBNA-2
4.3 0.004 Wp
5.4 0.042 A73
6.1 2x10-4 BHRF1
11.6 9x10-6 EBNA-3B
22.6 10-8 Unknown
23.2 2x10-7 EBER2
Fold
≤ -2
-1.5
-1.2
-1.1
±1
1.1
1.2
1.5
≥ 2

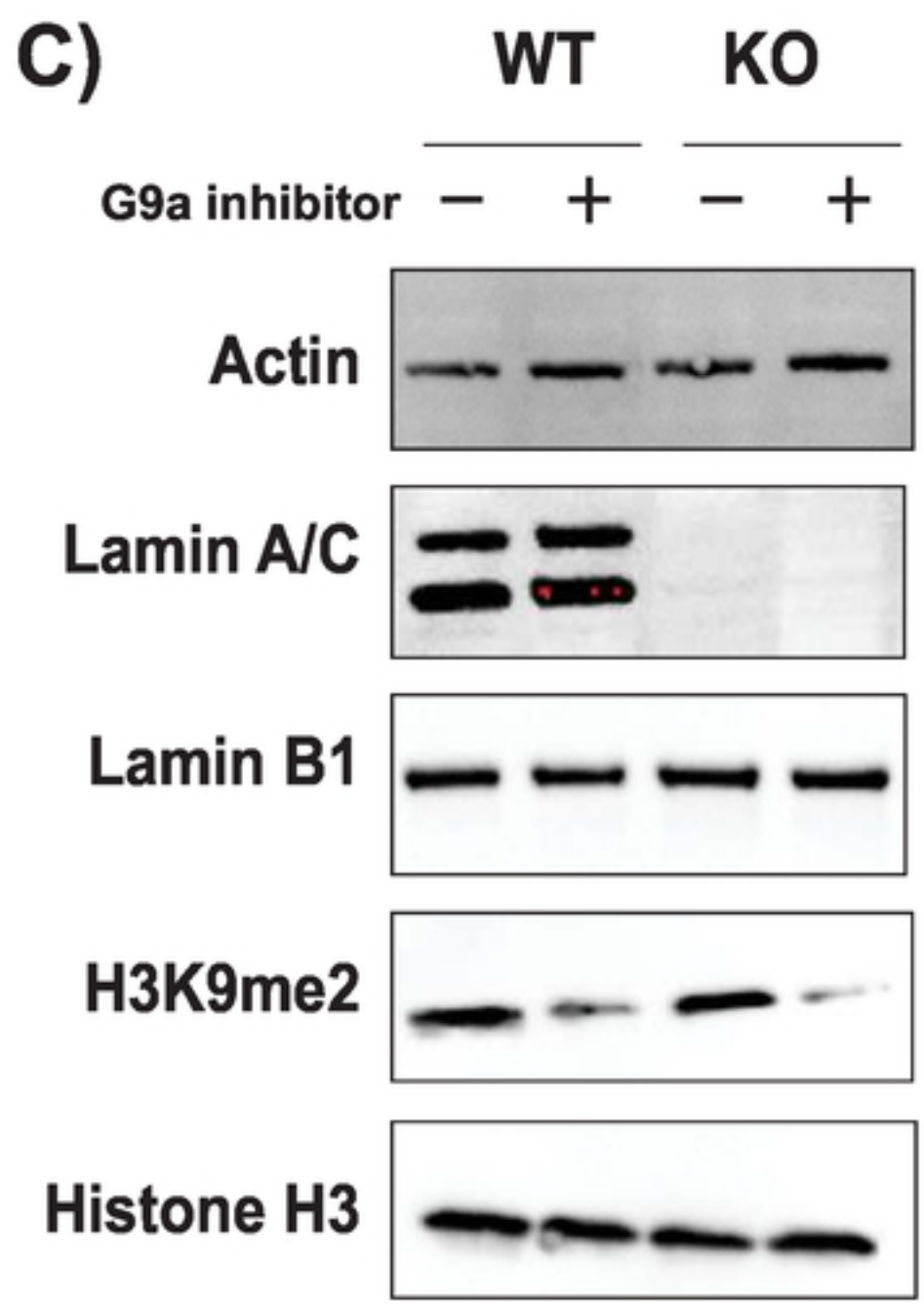
C)
WT
KO
G9a inhibitor
−
+
−
+
Actin
Lamin A/C
Lamin B1
H3K9me2
Histone H3

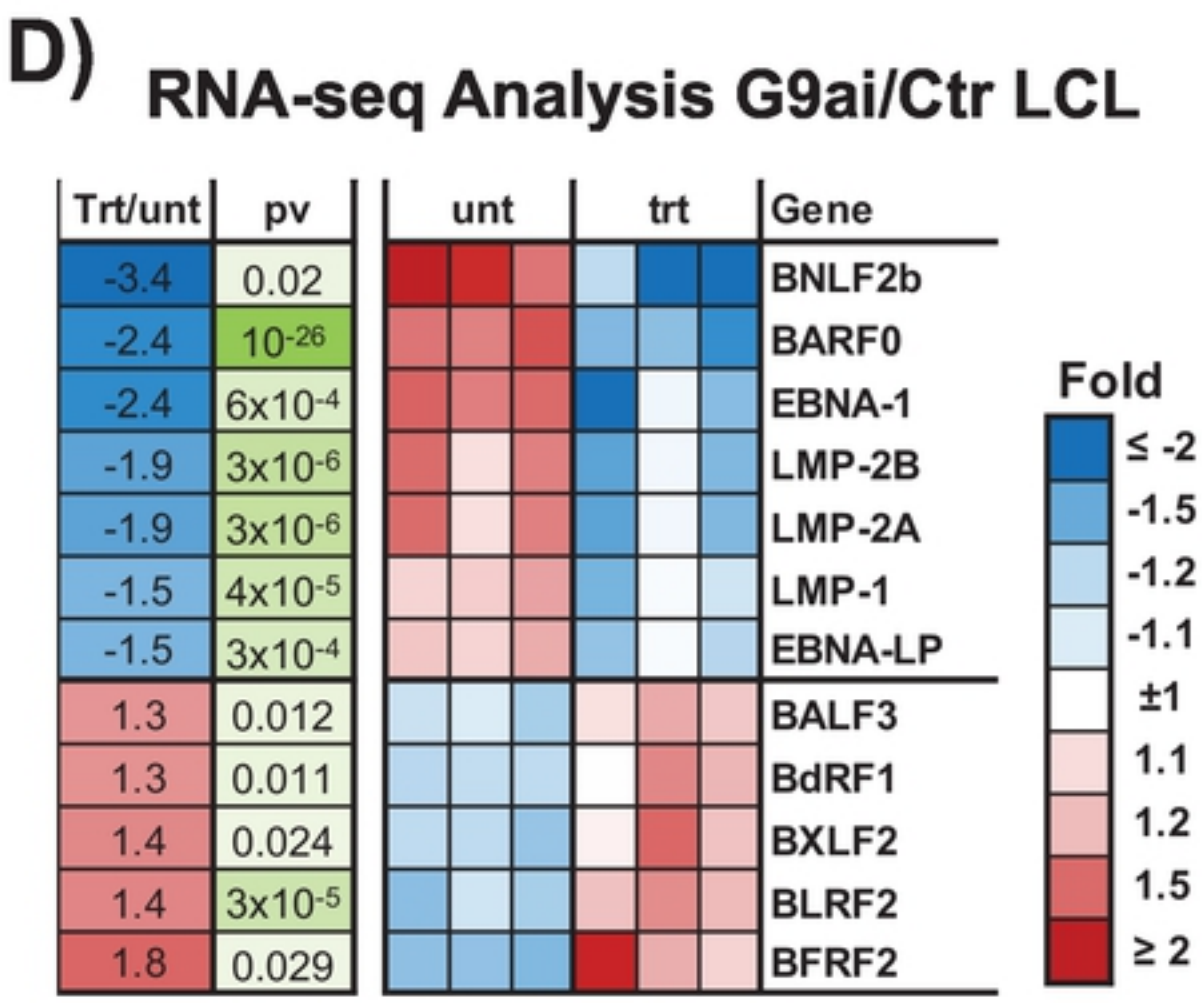
D)
RNA-seq Analysis G9ai/Ctr LCL
Trt/unt
pv
unt
trt
Gene
-3.4 0.02 BNLF2b
-2.4 10-26 BARF0
-2.4 6x10-4 EBNA-1
-1.9 3x10-6 LMP-2B
-1.9 3x10-6 LMP-2A
-1.5 4x10-5 LMP-1
-1.5 3x10-4 EBNA-LP
1.3 0.012 BALF3
1.3 0.011 BdRF1
1.4 0.024 BXLF2
1.4 3x10-5 BLRF2
1.8 0.029 BFRF2
Fold
≤ -2
-1.5
-1.2
-1.1
±1
1.1
1.2
1.5
≥ 2

Figure 7

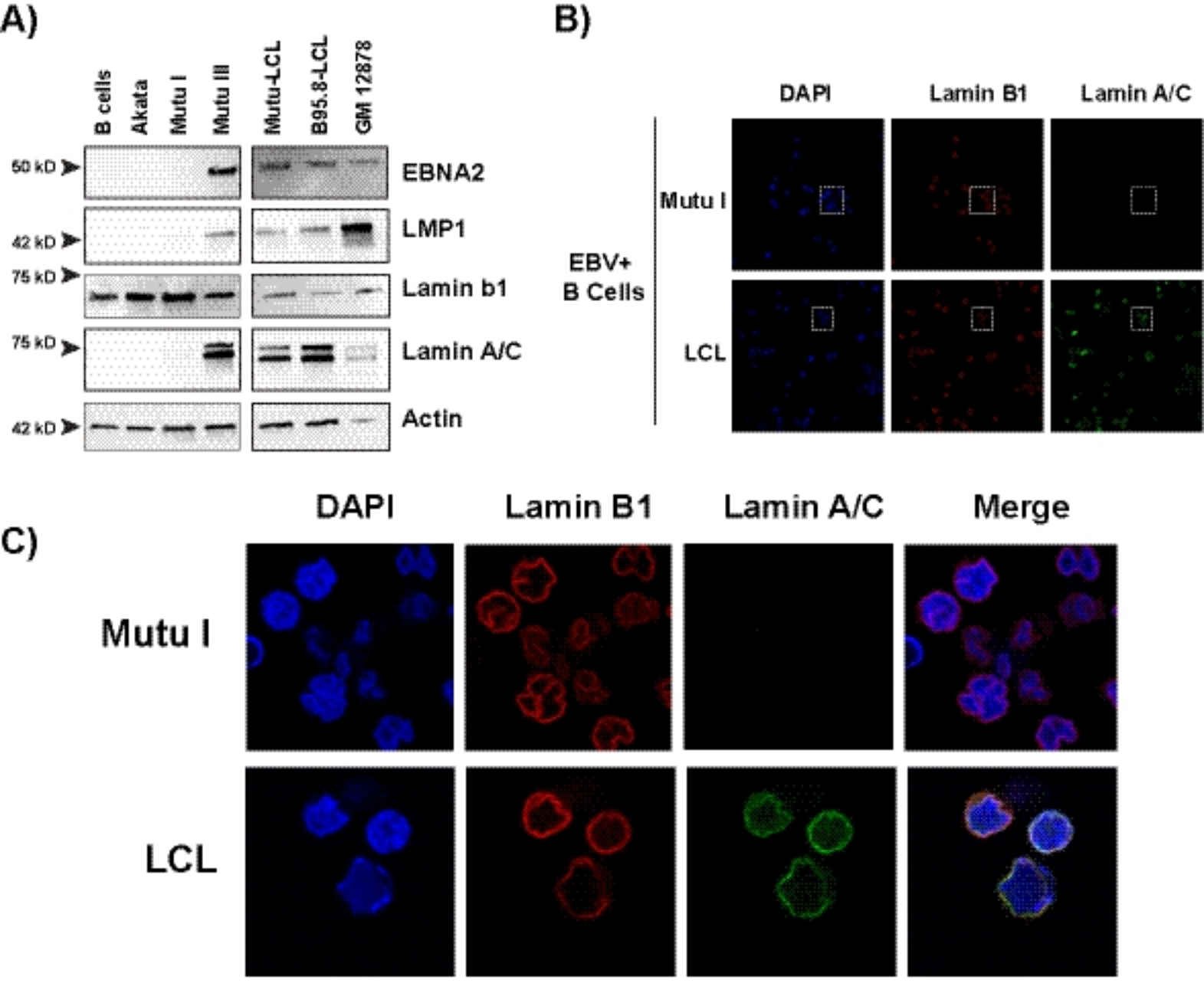
A)
B cells
Akata
Mutu I
Mutu III
Mutu-LCL
B95.8-LCL
GM 12878
50 kD
42 kD
75 kD
75 kD
42 kD
EBNA2
LMP1
Lamin b1
Lamin A/C
Actin
B)
DAPI
Lamin B1
Lamin A/C
EBV+
B Cells
Mutu I
LCL
C)
DAPI
Lamin B1
Lamin A/C
Merge
Mutu I
LCL

Figure 1